---

**Article:**
Palivec, Vladimír, Viola, Cristina M, Kozak, Mateusz et al. (8 more authors) (2017) Computational and Structural Evidence for Neurotransmitter-mediated Modulation of the Oligomeric States of Human Insulin in Storage Granules. The Journal of biological chemistry. pp. 8342-8355. ISSN: 1083-351X

https://doi.org/10.1074/jbc.M117.775924

---

# Computational and Structural Evidence for Neurotransmitter-mediated Modulation of the Oligomeric States of Human Insulin in Storage Granules

**Vladimír Palivec[‡], Cristina M. Viola[§], Mateusz Kozak[§§], Timothy R. Ganderton[§], Květoslava Křížková[‡], Johan P. Turkenburg[§], Petra Halušková[‡], Lenka Žáková[‡], Jiří Jiráček[‡*], Pavel Jungwirth[‡*], Andrzej M. Brzozowski[§*]**

From York Structural Biology Laboratory, Department of Chemistry, The University of York, Heslington, York YO10 5DD, United Kingdom[§], Institute of Organic Chemistry and Biochemistry, Academy of Sciences of the Czech Republic, v.v.i., Flemingovo nám 2, 166 10 Prague 6, Czech Republic[‡]

Running title: *Structural forms of storage insulin in pancreas*

[*]To whom correspondence should be addressed: Andrzej M. Brzozowski, York Structural Biology Laboratory, Department of Chemistry, The University of York, Heslington, York YO10 5DD, United Kingdom[§], E-mail: marek.brzozowski@york.ac.uk; Telephone: +44-1904-328265; FAX: +44-1904-328266; or to Pavel Jungwirth or Jiří Jiráček, Institute of Organic Chemistry and Biochemistry, Academy of Sciences of the Czech Republic, v.v.i., Flemingovo nám 2, 166 10 Prague 6, Czech Republic[‡]; Telephone: +420220410314 or +420 220 183 441; E-mail: pavel.jungwirth@uochb.cas.cz or jiracek@uochb.cas.cz.

**Keywords:** insulin, pancreatic islet, vesicles, serotonin, dopamine, crystal structure

**ABSTRACT**

**Human insulin is a pivotal protein hormone controlling metabolism, growth and ageing, and whose malfunctioning underlies diabetes, some cancers and neuro-degeneration. Despite its central position in human physiology, the *in vivo* oligomeric state and conformation of insulin in its storage granules in the pancreas are not known. In contrast, many *in vitro* structures of hexamers of this hormone are available, which fall into three conformational states: $T_6$, $T_3R^f_3$ and $R_6$. As there is strong evidence for accumulation of neurotransmitters, such as serotonin and dopamine, in insulin storage granules in pancreatic β-cells, we probed by molecular dynamics (MD) and protein crystallography (PC) if these endogenous ligands affect and stabilize insulin oligomers. Parallel studies independently converged on the observation that serotonin binds well within the insulin hexamer (site I), stabilizing it in the $T_3R_3$ conformation. Both methods indicated serotonin binding on the hexamer surface (site III) as well. MD, but not PC, indicated that dopamine was also a good site III ligand. Some of the PC studies also included arginine, which may be abundant in insulin granules upon processing of pro-insulin, and stable $T_3R_3$ hexamers loaded with both serotonin and arginine were obtained. The MD and PC results were supported further by in solution spectroscopic studies with R-state specific chromophore. Our results indicate that the $T_3R_3$ oligomer is a plausible insulin pancreatic storage form, resulting from its complex interplay with neurotransmitters, and pro-insulin processing products. These findings may have implications for clinical insulin formulations.**

Insulin is one of the key human protein hormones that is responsible for the maintenance of metabolic homeostasis, with an influence on cell proliferation and regulation of ageing (1,2). Defects in insulin bio-availability, or impaired insulin receptor signalling, lead to different pathological conditions, such as diabetes (3-5), cancers (6-8) and Alzheimer's disease (9).

Insulin is a 51 amino acid protein consisting of two disulphide-linked chains (A1-A21, B1-B30), and exerts its functions through binding as a monomer to the $(\alpha\beta)_2$ hetero-dimer Tyrosine-Kinase type insulin receptor (IR) (10,11). Insulin is produced from a single chain pro-insulin, and stored in pancreatic β-cells in storage granules (termed large dense core vesicles; LDCV), from which it is released into the bloodstream in response to elevated blood glucose levels. The first 3-D crystal structure of insulin was described by D.C. Hodgkin's group in 1969 (12), in the form of its hexameric assembly (with three and two-fold rotational symmetry (i.e. trimer of dimers),

obtained in the presence of $Zn^{2+}$ ions. Two $Zn^{2+}$ ions were identified in the hexamer on its three-fold axis, being coordinated by three imidazole side chains of HisB10. This, and subsequent similar findings resulted in a generally accepted paradigm that the hexamer is the storage form of insulin in LDCV in pancreatic β-cells, while upon its release into the bloodstream it dissociates to monomers which represent the active form of the enzyme (13). The pioneering work of D.C. Hodgkin was followed by 3-D descriptions of hundreds of *in vitro*-studied insulin hexamers, dimers, and monomers (for reviews see for example (14-16). However, the actual *in vivo* storage form of insulin in pancreatic β-cells LDCVs is still not known, and it is extrapolated from its *in vitro* structures. Surprisingly, there are more advances into the very elusive nature of insulin:IR interactions (17,18), than into the *in vivo* form of this hormone, investigation of which presents formidable experimental challenges.

The *in vitro* data showed that insulin hexamers can be grouped into three structurally distinct states/families: $T_6$, $T_3R^f_3$ and $R_6$ (15,16), which differ by the conformation of the B1-B6 N-termini of hormone's B-chain (see Figure 1 and Figure S1). In the $T_6$ hexamers, the initial B1-B6 segments of the B-chains are fully extended, followed by B7-B10 type II' β-turns that go into invariant B9-B19 α-helices. In contrast, the B1-B6 segments acquire an α-helical conformation in the R-state, extending the B9-B19 α-helix (19). The insulin $R^f_3$ state is similar to the α-helical $R_6$ state, however, the long R-state B-chain helix is shortened to the B3-B19 segment, while the B1-B3 residues depart ("fray") from the α-helical fold (20,21). The $TR^f$ transition can be induced by an increase of, for example, the concentration of $Zn^{2+}$, $SCN^-$, and $Cl^-$ ions (22), or by the presence of phenolic derivatives (e.g., phenol or similar small cyclic alcohols) at low concentrations (23-25). The $R^fR$ (or full TR), transition can be accomplished by a further increase of the concentration of phenolic ligands (19,24). The octahedral $Zn^{2+}$-coordination is also a signature of the T-state (assured by three HisB10 imidazoles and three water molecules), while the $Zn^{2+}$ tetrahedral coordination (three HisB10 and, for example, a $Cl^-$ ion) is typical for the $R^f$/R-states (e.g. (26)). This coordination switch results from a smaller space above the $Zn^{2+}$ ion in the R-state that is obstructed there by a longer B1-B8 helical part of the B9-B19-helix, and a newly formed binding pocket for cyclic alcohols on the dimer interface, formed by the side chains of A6-7, A9-11, A16, B7, B11, and B5-7 (the so-called site I, or phenol main-binding site) However, variations of the $Zn^{2+}$ coordination spheres are also observed frequently (27).

Although site I is the main binding cavity for all phenol-like ligands, they have also been identified in other regions of the hexamers; e.g. site II, formed by side chains B9, B12, B16, B17, B9, B10, B13, site I/II: B10, B14, B16, B17 and B9 (28). Hexamer-surface-exposed (between insulin dimers) phenolic site III (A14, A17) has been observed as well (29). The serendipitous character of the discovery of the phenol-stabilised R-state resulted from the bactericide like applications of phenol in clinical formulations of insulin. Nevertheless, the R-like states of the hormone have clinical importance, as the $R^f$/R-trimers/hexamers are more stable (30). This is mostly due to the slower $Zn^{2+}$-solvent exchange, which results in a higher hexamer-monomer dissociation constant. However, the physiological relevance of T/$R^f$/R-states for an effective insulin:IR binding, and for the storage form of the hormone (e.g., protection against proteolysis), is still unknown.

Here, we attempt to shed light on a possible conformation of the *in vivo* storage form of insulin in insulin-containing granules in pancreatic β-cells. Although the exact chemical composition of LDCVs still awaits full characterisation, they contain $Zn^{2+}$ ions and phenolic neuro-transmitters such as dopamine and serotonin, which are involved in regulation of exocytosis of the granules and insulin release (31-33). Therefore, we hypothesise that both neurotransmitters can bind to, and affect the structure of, insulin hexamers, assembled in the presence of zinc cations. We probe these effects in parallel via molecular dynamics simulations (MD) and protein X-ray crystallography (PC). These were further supplemented by spectroscopic studies with the use of a sensitive chromophore, 4-hydroxy-3-nitrobenzoic acid (4H3N), which specifically binds to R-state insulin as indicated by a red-shift of its absorption spectrum. Moreover, as arginine can accumulate in LDCVs upon processing of pro-insulin at its two Arg-rich sites (34,35) and as arginine-rich poly-peptides (spermine/spermidine)

are used in some insulin injections formulations (36,37), we also probe the structural effect of this amino acid on insulin oligomeric assembly.

Both the MD and X-ray serotonin-related studies point to a stable insulin hexamer-serotonin-site I complex and its dynamic association with site III. Both methodologies excluded dopamine binding in site I. MD simulations also indicate preferential dopamine over serotonin binding to site III, while solid-state X-ray analyses yields only serotonin site III complexes.

In addition, crystal structures of serotonin-insulin hexamers loaded with arginine have been obtained that underline a possible more complex, physiological role of insulin-arginine interactions.

Results concerning site I complexes are corroborated by 4H3N spectroscopic experiments, which provide apparent binding constants for interaction of insulin hexamers with phenolic ligands and arginine. Our findings thus provide a novel insight into the storage mechanism of insulin in pancreatic β-cells, being also relevant for novel insulin formulations for clinical applications.

**RESULTS**

*MD simulations of serotonin, dopamine, and phenol binding in site I* - Here, we address the question of whether two neurotransmitters, serotonin and dopamine, can substitute phenol in its insulin $R_6$ hexamer binding site I. MD simulations were performed for the $R_6$ insulin hexamer, where site I-bound phenol was systematically replaced with neurotransmitters (each ligand in two steric-clash-free orientations, see Figure 2). As expected, the MD simulations yielded the benchmark phenol-bound insulin $R_6$-state hexamer ($InsPheR_6$) with a low root mean square deviation (rmsd) of ~1.6-1.8 Å from the reference $InsPheR_6$ structure, indicating that the system does not deviate significantly from the NMR structure during the simulation (Figure 3).

Both serotonin ($InsSerR_6$) and dopamine ($InsDopR_6$) complexes with ligands orientation(1) behaved similarly to $InsPheR_6$, with the backbone rmsd just above 2 Å. However, the starting orientation(2) of the ligands led to higher rmsds of ~2.8 Å (Fig. 2) indicating somewhat larger structural changes. A more direct insight into the behavior of the ligand in site I can be obtained from a direct comparison of their rmsds while hydrogen-bonded (HB) to the backbone carbonyl CO of CysA6 (Fig. 4).

The MD simulations confirm that phenol molecules are essentially fixed in site I with a minimal dynamic behavior. Two of the six phenols transiently break HBs (both with CysA6 and CysA11), however, they remain in site I, eventually re-establishing the original geometry of binding. Similarly, all but one of the serotonin molecules in the starting conformation(1) stay in site I (only one serotonin ligand temporarily leaves this cavity). However, serotonin in starting geometry(2), as well as dopamine in both starting orientations, break most of the crucial hydrogen bonds. Serotonin, but not dopamine, thus essentially mimics phenol interactions observed in $InsPheR_6$ with its charged aminoethyl-group forming HB with backbone carbonyl CO of CysA11, fitting well into the binding site I.

The strength of binding (i.e., the binding free energy and the corresponding dissociation constant) of phenol and the two neurotransmitters, was calculated using the thermodynamic integration method (see Table 1).

The free energy calculations confirmed and quantified the pattern observed in direct MD simulations, indicating a similarly strong binding of phenol and serotonin to site I ($K_d$ of $5.4\times10^{-4}$ M and $8.1\times10^{-4}$ M, respectively), as well as demonstrating a lack of any stable conformation of dopamine in this cavity (reflected in a positive binding free energy).

*MD simulations of serotonin and dopamine probing the hexamer surface sites* - Initial simulations of the $R_6$ insulin hexamer with six dopamine molecules located in the phenolic pockets indicated that dopamine does not bind strongly to the phenolic pocket. At the same time, several dopamine molecules left the phenolic pocket to bind to the hitherto unexplored site III at the surface of the insulin hexamer. Therefore, an additional set of calculations was performed to characterize the binding of neurotransmitters to the surface of the insulin $R_6$ hexamer (for simulation details see SI). These simulations showed that dopamine binds at three equivalent binding sites in-between the symmetry-related dimers (Figure 5, top), which correspond to the previously sporadically observed site III. Analogous MD simulations for serotonin showed a similar mode of

binding in site III, but with a spatially looser neurotransmitter distribution, which reflects its weaker binding to this site compared to dopamine (Fig. 5, bottom). Finally, the binding of neurotransmitters at the surface sites has only a minor effect on the structure of the hexamer.

Both dopamine and serotonin bind in site III in a pocket between GluA17 and Tyr14 from neighboring dimers (Figure 6). The stronger binding of dopamine over serotonin shown by free energy calculations (*vide infra*) results from its interactions with TyrA14, a hydrogen bond of the phenolic OH to GluA17, and a salt bridge between the aminoethyl group and the carboxylic group of GluA17. Similar interactions are present for serotonin; however, the steric fit is not as good as for dopamine. Dopamine, serotonin, and phenol binding in site III were quantified by evaluation of the binding free energies and the corresponding dissociation constants (Figure 7 and Table 2) using the umbrella sampling method, with symmetry and volume entropy corrections.

In contrast to site I, dopamine is the strongest binder to site III ($K_d$ $4.38\times10^{-3}$ M), with serotonin and phenol showing a much weaker affinity for this surface site ($K_d$ of $2.13\times10^{-1}$ M and $2.59\times10^{-1}$ M, respectively).

*Insulin-serotonin crystal complex* – The crystal structure of insulin grown in the presence of serotonin and $Zn^{2+}$ revealed a $T_3R_3$ hexamer (referred to here as $InsSerT_3R_3$), with six neurotransmitters and two $Zn^{2+}$ ions per hexamer (Figure 8). The minimum serotonin concentration that still yielded complex crystals was within the 35-40 mM range. The asymmetric unit of this crystal contains 14 molecules of insulin hence providing reliable, independent multi-copy structural evidence. The hexamer quaternary structure is indeed $T_3R_3$ as the B1-B3 N-termini acquire here a more R-like (fully α-helical) fold, rather than an $R^f$, 'frayed', conformation observed in $T_3R^f_3$ oligomers.

Coordination of both $Zn^{2+}$ ions is tetrahedral, regardless of the R or T protein environment, with axial $Cl^-$ ligands. The overall fold of $InsSerT_3R_3$ is very similar to other $T_3R^f_3$ hexamers. For example, the rmsds of $InsSerT_3R_3$ from complexes with phenol (PDB ID: 1MPJ (29)), Tylenol (1TYL (23)), paraben (MTH (29)), 4-hydroxy-benzamide (1BEN (25)) are 0.8911 Å, 0.9886 Å, 0.9105 Å, and 1.1570 Å, respectively.

Also, this hexamer is not significantly different from phenol-free $T_3R^f_3$ hexamers induced by ions such as $SCN^-$ (2TCI(29) - rmsd 0.9919 Å) and $Cl^-$ (1G7A(38) - rmsd 0.7765 Å).

Serotonin occupies six sites in $InsSerT_3R_3$: three phenol 'main' sites I, and three hexamer surface sites III. It is tethered (Figure 9) into site I *via* (typical for phenolic ligands) HBs of its OH group to –CO of CysA6 (range of 2.41-2.43 Å), and to –NH of CysA11 (2.93-3.17 Å); a weaker HB –OH contact to –CO of SerA9 (3.38-3.41 Å) further stabilizes this phenolic anchor. A significant HisB5-Nε2..π pyrrole HB (3.46-3.56 Å) contributes to the immobilization of the serotonin indole ring, which is assisted further by more subtle van der Waals (hydrophobic) interactions, especially with LeuB17 (3.45-3.59 Å). The aminoethyl side chain of serotonin points towards the surface of the hexamer, i.e., into the space/gap between two 3-fold related dimers. The –NζH amino group of this side chain is hydrogen bonded to Oε1 of GluB21 (2.55-2.75 Å) and −CO of CysA11 (2.72-2.79 Å).

In contrast to site I, the serotonin-binding mode to site III is rather dynamic, indicating its mobility on the $InsSerT_3R_3$ surface. Although serotonin is pincered there in a hydrophobic clamp of TyrA14 (π..π interactions ~3.5 Å), and the side chain of LeuA13 (from a symmetry related dimer), the ligands' electron density is generally less well defined there. The serotonin phenolic OH group makes HBs to the Oεs atoms of GluA17 (2.96-3.44 Å), and it can be stabilized by water-mediated HB to the hydroxyl of TyrA14. The HBs of the GluA17 carboxylic side chain to the guanidinium group of ArgB22 (2.75-2.82 Å) contributes further to the structural stability of the serotonin-OH environment. However, it is evident that the aromatic moieties of Tyr14 and serotonin can slide parallel to each other, indicating further adaptability of this mode of binding. Relative flexibility of site III is also seen in different modes of the HB network to the –Nζ group of the serotonin aminoethyl side chain. It is engaged primarily by HBs to the carboxyl side chain of GluA17 (2.65-2.76 Å), and *via* a water molecule to ArgB22, but this network of HBs is prone to disruption due to the flexibility of the serotonin

surface-exposed side chain. In summary, the GluA14/ArgB22-pair are the two-fold symmetry-related providers of HBs to serotonin (one pair to the ligand's OH group – the other one to the end of its side chain) in site III, but these HB-networks are not fully symmetrical in overall geometry and strength due to a non-symmetrical ligand in this site. The swing of the other (not involved in serotonin binding) TyrA14 side-chain, away from site III, breaks down the two-fold symmetry of this interface even further. Finally, we note that all our dopamine:insulin co-crystallizations were unsuccessful, likely due to the oxidation of the ligand, despite the inclusion of some anti-oxidation agents in the media.

*Insulin-serotonin-arginine crystal complex* - A similar set of crystallization conditions yielded crystals of insulin in a ternary complex with serotonin and arginine (referred to here as $InsSerArgT_3R_3$). Arginine- and $Zn^{2+}$-containing crystallizations of insulin were carried out in the presence, and absence, of the previously established optimum serotonin concentration (40 mM). Serotonin-arginine containing solutions yielded several morphologically different – but crystallographically very isomorphous – crystal forms. Despite their similarity, two of these forms (f1, f2) (referred to as $InsSerArgf1\text{-}T_3R_3$ and $InsSerArgf2\text{-}T_3R_3$) are reported here due to a dynamic (i.e. with high level of disorder) nature of Arg:insulin binding, hence the need for more independent structural evidence about the nature of these interactions.

Both InsSerArg complexes appear in the $T_3R_3$ hexamer state, with all $Zn^{2+}$ ions in a tetrahedral coordination with $Cl^-$ as an axial ion. They are very similar to the $InsSerT_3R_3$ complex, with overall rmsd of 0.2193/0.2349 Å between these structures.

Despite the presence of arginine, the serotonin modes of binding in sites I are practically the same as in the Ins-Ser complex (Figure 10). However, the site III shows more significant structural variety in binding of this neurotransmitter. Some serotonins in site III are bound in a fashion observed in $InsSerT_3R_3$, however, some of these ligands are flipped in both $InsSerArgT_3R_3$ crystal forms, i.e., the –OH and aminoethyl groups switch their positions. As both of them benefit from a similar HB network of symmetrical GluA14/ArgB22 tandems, the overall HB-connectivity is conserved here as well, with the exception of the Nζ atom of the aminoethyl side chain. It forms, in some sites III, a new HB with the hydroxyl group of TyrA14 (2.67 Å), besides maintaining a HB to the side-chain of GluA14 as well.

It has to be stressed, that several serotonins in site III and arginine molecules (see below) in the $InsSerArgT_3R_3$ complex have been refined with half-occupancies and, in some cases, with more arbitrary modeling due to their partial definition in the electron density maps. This reflects the dynamic and mobile character of some ligand:hormone interactions in $InsSerArgT_3R_3$ hexamers.

Arginine molecules occupy the 'T-state-half' of the trimer (Figure 11), with their Cα-moieties being part of the T-state trimer surface (on the level with the $Cl^-$ ion), while their side chains point towards the hexamer core, relatively parallel to its central axis. The aminocarboxy-Cα groups of Arg have been modeled in both $InsSerArgT_3R_3$ forms with some flipped/alternative conformations around the Cα atom.

The dominant stabilizations of the Arg Cα-end result from HBs of the carboxyl group to the NH of CysB7 (2.76-3.31 Å), and amino acid amine group to CO of HisB5 (2.86-3.18 Å). However, it is possible to model this part of arginine with alternative conformations; a likely effect of a dynamic character of these ligands at the wider, and more solvent accessible, $T_3$-side of the hexamer.

In contrast, the HBs of the Arg guanidinium groups are much better defined, especially in the $InsSerArgf2T_3R_3$ form. One of their main signatures is the extensive HB network with both GluB13 and HisB10 residues. Here, the GluB13 Oε1/Oε2 atom forms HBs to Arg Nη1 (2.11-2.33 Å) and Nδ1 of HisB10 (2.82-3.14 Å), while the second Nη2 atom of the guanidium group is HB-ed to CO of HisB10 as well (2.71-2.82 Å). The last guanidinium Nε1 atom locks this group by HB to the hydroxyl Oγ of SerB9. Some of these HBs are broken in the $InsSerArgf1T_3R_3$ form, indicating also the increased mobility of this environment, especially some shifting of the arginine parallel to the hexamer 3-fold axis.

*Determination of ligands' $K_d$ values by solution 4-hydroxy-3-nitrobenzoic acid (4H3N) assay* - The interactions of insulin hexamers with phenol, serotonin, dopamine, and arginine in solution were investigated and quantified by spectroscopic studies, with the 4-hydroxy-3-nitrobenzoic acid (4H3N) chromophore, which binds exclusively to HisB10 sites in the R-state only, which is associated with the red-shift of its absorption spectrum. This allows for the determination of the apparent binding constants ($K_d$) of selected ligands to insulin hexamers, and estimation of the values of their maximum specific binding ($B_{max}$), which can be considered here as a measure of the amount of the R state induced by the ligand. In addition, the Hill coefficients (*h*) that indicate the scale of cooperativity (likely very complex) between ligand and/or insulin its hexameric state upon ligand binding, were evaluated as well.

First, we determined the change in 4H3N absorption upon titration of selected ligand to $T_6$ insulin hexamer pre-incubated with this chromophore. Fitting of all curves (Figure 12) gave $K_d$, $B_{max}$, and *h* values (Table 3) for all types of experiments. The data from Table 3 are also presented in a bar plot in Figure S2. The 4H3N spectroscopic data indicate that phenol is the strongest binder to insulin hexamers; about four times stronger than serotonin ($K_d$ values of 0.85 mM and 3.34 mM, respectively, see Table 3). In contrast, titration of the same $T_6$ insulin hexamers by arginine and dopamine did not induced any changes in the 4H3N absorption spectra (data not shown), indicating a lack of binding to site I and, subsequently, inability to induce $T_6 \rightarrow T_3R_3/R_6$ transitions.

Addition of phenol or serotonin to insulin/4H3N that was also pre-incubated with 5 mM Arg resulted, however, in different patterns of binding curves (Figures 12C and 12D), compared to sole ligands:insulin/4H3N titrations (Figures 11A and 11B). Similar trends were observed for phenol and serotonin titrations of insulin/4H3N pre-incubated with 5 mM dopamine (Figures 11E and 11F). It seems that in both cases the pre-incubation of insulin/4H3N with arginine or dopamine (which are no hormone Site I binders on their own) lowers the phenol $K_d$ to 0.75 and 0.64 mM, respectively. In contrast, arginine and dopamine do not change the binding affinity of serotonin to insulin hexamers (Table 3, Figure 12A).

The higher $B_{max}$ value for phenol than for serotonin (0.17 vs 0.11) may also indicate that serotonin is not able to fully induce the $R_6$ state of the hexamers. Note that pre-incubation of insulin/4H3N with arginine or dopamine lowers the $B_{max}$ values of phenol or serotonin binding to insulin (Figure 12B). The Hill coefficient of phenol binding to insulin hexamers (Figure 12C) is also higher ($h$ = 2.2) than that for serotonin (1.6) indicating a lower degree of cooperativity for serotonin-insulin interactions. Interestingly, the presence of arginine or dopamine lowers cooperativity (i.e., the *h* value) of phenol-insulin binding, but increases the *h* value for serotonin interactions with the hormone. This effect seems to be even more noticeable in the case of dopamine ($h$ = 7.1) but these data are accompanied by a high experimental error (see Table 3 and Fig. S2).

## DISCUSSION

Our parallel and independent MD simulations, X-ray crystallography, and ligand binding experiments provide a concise picture showing that the insulin hexamer can accommodate, and be affected by, ligands that are present in the hormone storage LDCV granules in pancreatic β-cells. These ligands can be of exogenous origin, such as neurotransmitters (serotonin or dopamine) involved in regulation of insulin secretion, or they can be by-products of pro-hormone/pro-insulin processing (e.g., arginine) that accumulate in the granules.

All the above methods indicated that serotonin is a good phenol-compatible ligand for insulin hexamer site I, while dopamine is not a site I binder. Serotonin site-I binding engages its phenolic OH in 'phenol-canonic' HBs to CO of CysA6 and NH of Cys A11. This is despite a ~29° tilt of its indole plane with respect to the phenol benzene ring - a movement of the aromatic moiety that is also observed (to a different degree) in tylenol (23), paraben (29), and benzamide (25) complexes. However, the side chains of the latter phenolic ligands are oriented towards the central channel of the hexamer, while the aminoethyl group of serotonin points into the opposite direction, i.e., towards the surface of the hexamer. This results in further enhancement of serotonin stability in site I by fixing its side chain via HBs

with the CO of Cys A11 and carboxyl of GluB21. The fitting of serotonin in site I is completed with a strong HisB5–Nε2..π-pyrrole contact. The firmness of serotonin-site I interactions, which is propagated likely towards the N-termini of the B-helix, combined also with a very good overall fit of serotonin into site I may be behind the induction of the R (i.e., not $R^f$) conformation of the $T_3R_3$ hexamer. This is rather unique, as this type of insulin quaternary arrangement occurs mainly in the $T_3R^f_3$ state. $T_3R_3$ hexamers were observed only within a $R_6 \rightarrow T_3R_3$ retrograde conformational change (39-41) upon evaporation of phenol from $R_6$ insulin crystals, which is a process that cannot occur for the non-volatile serotonin ligand. Therefore, the stability of the $SerInsT_3R_3$ complex may indicate that this hormone's conformer is indeed close to its putative native form in pancreatic LDCV (as postulated, for example, by Dunn et al. (26)). Moreover, larger $B_{max}$ and Hill coefficient *h* values (obtained from 4H3N spectroscopy studies) for phenol as compared to serotonin suggest that the latter, despite its 'perfect' fit into site I, cannot fully induce the insulin $R_6$ state (as also confirmed by the lack of $R_6$ serotonin hexamer crystals even at a very high ligand concentration). These findings corroborate further the potential physiological aspect of the $T_3R_3$ insulin conformer as the only possible oligomeric species in the presence of serotonin. Although MD simulations did not exclude the presence of a stable $SerInsR_6$ conformer, the $R_6$ state was postulated in the MD work *a priori* (due to its thermodynamic superiority in the presence of phenol ligands) to identify the potential ligand-binding sites rather than to investigate the impact of a particular ligand on the state of the insulin hexamer.

The lack of stable site-I-dopamine complexes was demonstrated by all methods employed in this study. It seems that this is not due to a steric ligand-cavity incompatibility, as the dopamine dispersion contribution to free energy of binding in the MD simulations is more negative compared to phenol. Rather, as the superposition of dopamine with phenol or serotonin ligands in site I suggests, the lack of dopamine binding is due to an electrostatic mismatch, namely its inability to accommodate the charged aminoethyl side chain in the site I cavity. The smaller aromatic scaffold of dopamine thus does not allow its side chain to reach the hexamer surface and form HBs observed in serotonin complexes.

As the 4H3N spectroscopic applicability was limited here to the environment of HisB10 and hence the site I, the evidence for other insulin sites-ligands interactions came solely from MD simulations and X-ray crystallography. Both showed serotonin binding to surface site III, while only MD calculations predicted the possibility of a stable site III-dopamine complex (note, however, that dopamine-insulin co-crystallization may be hampered by a rapid chemical degradation/oxidation of dopamine). Interestingly, MD calculations indicated superior dopamine binding to site III, with its $K_d$ ~50 times better than for phenol or serotonin. MD-predicted dopamine's dominance at site III is interesting, as these simulations show its binding in a similar mode to serotonin-site III complex, which is observed both in MD simulations and crystal structures. Both neurotransmitters engage TyrA14 and GluA17/ArgB22 side chains from 2-fold symmetry related dimers in the network of HBs and π..π stacking interactions. Moreover, crystal structures of $InsSerT_3R_3$ underline also the dynamical character of site III-mode of binding, which involves flipping of the serotonin indole ring (i.e., swapping positions of –OH and the aminoethyl side chain), and a certain variability of the TyrA14-OH/GluA17/ArgB22 HB patterns.

The impact of these ligands, which are natural components of pancreatic β-cells insulin-storing LDCVs was also extended from neurotransmitters to probing of arginine-insulin hexamer interactions. It has been postulated earlier that arginine can accumulate in these granules upon processing of pro-insulin at its two sites (Arg31-Arg32 and Lys64-Arg65) (34,35), which are cleaved by specific convertases during maturation of this hormone (42,43). Here, the X-ray crystallography revealed that arginine can penetrate serotonin-containing hexamers ($InsSerArgT_3R_3$) without significant changes to their $InsSerT_3R_3$ state. Arginine is accommodated there in channels within the $T_3$ trimer, parallel to the hexamer 3-fold axis and opposite to $R_3$ trimer's sites I filled by serotonin, which leads to filling the voids around $Zn^{2+}$ and His B10. Binding of arginine in $InsSerArgT_3R_3$ is dynamic with high mobility and alternative, slightly different ligand

conformations. The flexibility of arginine is concentrated mostly around its $-C\alpha NH_2COO^-$ moieties, which form weak alternative HBs to main chain groups of CysB7 and HisB5, exhibiting also some flipping around the Cα atom. In contrast, the guanidinium groups of the arginines are firmly engaged in extensive networks of HBs, which link them with side chains of GluB13, side- and main-chain of HisB10, and the side chain of SerB9. This simultaneous binding of the two very different ligands to the $T_3R_3$ insulin hexamer, polarizes this oligomer even further into two structurally distinct trimers - $Arg_3T_3$ and $Ser_6R_3$. While Arg binding in the $ArgT_3$ trimer has a notable impact on the stability of the usually mobile GluB13 side chains, the solvent-exposed flexible $-C\alpha NH_2COO^-$ moieties may contribute to the disorder of the N-terminal parts of B-helices, which is, however, untraceable up to the HisB5 site in both arginine-containing and arginine-free serotonin complexes. In contrast, the GluB13 side chains are fully disordered in the $Ser_6R_3$ trimer, while the serotonins in sites I facilitate fixing of the B1-B19 helices in the R-state.

The structural partition of $Arg_3T_3$ and $Ser_6R_3$ is more complex. Firstly, although the site I pocket is mainly formed by two R-monomers, the T-state monomer contributes here also by LeuB17 and GluB21 towards serotonin aromatic rings and side-chain binding, respectively. Secondly, serotonin surface site III mediates also the structural interface between $T_3$ and $R_3$, as this binding site (formed by TyrA14/GluA17) is provided by the T- and R-monomers from the two-fold symmetry related dimers.

Interestingly, 4H3N spectroscopic data indicate that the presence of arginine increases (by ~13%) phenol (but not serotonin) affinity for site I and also increases the co-operative character of serotonin binding (as demonstrated by a higher Hill *h* factor). These structural and spectroscopic data provide evidence for the $T_3$-$R_3$ trimers cross-talk and, as postulated previously, for a heterotropic allostery within the insulin hexamer (22,30,44-47). However, the exact molecular detail behind this phenomenon has been elusive, likely involving a network of propagating longer range interactions, which fit the Seydoux, Malhotra, and Bernhard (SMB) cooperativity model (48). The stabilizing effect of guanidinium groups on GluB13-HisB10 and $Zn^{2+}$ may be one of the initial steps in this process, priming the other half of the hexamer for more effective serotonin binding (i.e., an element of the so-called half-site reactivity). The stability of $InsSerArgT_3R_3$ and $InsSerT_3R_3$ hexamers in the presence of physiological ligands, i.e., trapping of these oligomers in a stable $T_3R_3$ state, agrees also with the finding that conformational fluctuations of the $T_3$ trimer needed for the appearance of site I become constrained upon formation of $T_3R_3$.(49) This can be considered as one of the features of the negative cooperativity effect in the insulin hexamer, predicted by the SMB model as well.

The present 4H3N spectroscopic data also suggest a dopamine-lowering effect of phenol's $K_d$. As there is no evidence for dopamine site I-binding, this allosteric effect may result from longer-range cross-talk of the dopamine-site-III complex with the environment of site I. On the other hand, dopamine does not seem to significantly change the serotonin $K_d$, and therefore some 'competitive' crowding effect (e.g., dynamic occlusion of site I) between these two neurotransmitters cannot be excluded. It may also mean that dopamine-site-III binding facilitates the diffusion of a smaller ligand (i.e. phenol) into site I, while the increased stability of the insulin $R_3$-like trimer (via new HBs and interactions in site III) may obtrude its effect on binding of a larger ligand (such as serotonin).

It is worth mentioning that several tubular electron densities are also observed in $InsSerArgT_3R_3$ on the top of the $T_3$ trimer. These are linked with the modeled arginine ligands, suggesting the presence of more of these molecules on the hexamer surface, in the form of a HB-ing network of ligands. Some of this electron density is in contact with the $T_3$ $Zn^{2+}$ ion. Therefore, a contribution of the arginine $-COO^-$ group to the tetrahedral/monodentate coordination of $Zn^{2+}$ (observed also in the insulin $R_6$ structure (41)) cannot be excluded either. This direct arginine-$Zn^{2+}$ interaction would hamper the $T_3 \rightarrow R_3$ transition even further, thus reinforcing the stability of the $T_3R_3$ hexamer.

Arginine is widely used *in vitro* as a non-specific protein-folding stabilizing agent (49,50), and so its presence in $InsSerArgT_3R_3$ structures may reflect some of its physiologically relevant roles as a ubiquitous insulin ligand. Firstly, it may

serve as an unspecific, granules-abundant, insulin-folding stabilizer and hexamer half-life enhancer. Secondly, it may act as a more specific endogenous ligand that modulates the hexamer co-operativity, enhancing also the stability of its particular $T_3R_3$ storage form. This more specific role of arginine may result, among others, from its guanidinium counterion-like neutralization of the repulsive system of the GluB13 side chains in the hexamer core. Moreover, a simultaneous arginine-mediated cross-linking of GluB13 side chains with $Zn^{2+}$-binding HisB10, leading to stabilization of this structurally key region, further exemplifies the ligand-like role of this amino acid.

It has to be stressed, that insulin crystallization in the granules can be also affected by the intra-granular $Zn^{2+}$ concentrations, which are modulated by some $Zn^{2+}$ transporters (ZnT), especially by the disease-associated ZnT8 variants (51). However, the focus here was on insulin:neurotransmitter interactions, hence the experimental $Zn^{2+}$ concentrations (0.4 - 8mM) were maintained within typical insulin *in vitro* crystallization ranges. Interestingly, insulin crystallized here only in the form of $2Zn^{2+}$ hexamers, regardless the very high (25:1) $Zn^{2+}$:hormone molar excess in the crystals-yielding conditions.

There are ongoing efforts for a better insight into the size and content of insulin storage granules (e.g. (52)). Their exocytosis can also be morphologically and mechanistically quite heterogeneous (so-called 'kiss-and-run' phenomenon), releasing varying amounts and forms of granule content, and on different time scales (53). Therefore the final amount and form of insulin discharged to the circulation can be a very complex and multifactorial process; whether insulin:neurotransmitter:arginine hexamers are one of its variables, remains to be seen.

## CONCLUSIONS

We have demonstrated here that insulin oligomeric forms in storage granules in β-pancreatic cells, could be regulated by certain endogenous components of these vesicles, such as serotonin, dopamine and arginine. They are able to (i) shift the insulin oligomeric equilibrium towards the $T_3R_3$ state which, therefore, may be considered as the insulin storage form in pancreatic β-cells, (ii) affect and modulate the allostery of the insulin hexamer, (iii) may provide folding stability and protection for the insulin hexamer, and consequently (iv) may have a direct role in the modulation of insulin release from β-cells *in vivo*. Moreover, these ligands can act in a synergistic, heterotropic fashion, pointing to a co-operative, complex, and dynamic nature of the interactions within the insulin hexamer.

Therefore, the importance of the neurotransmitters for insulin beta-cell biology can be either cumulative, or even independent. Serotonin/dopamine are involved in the regulation of exocytosis of the granules, while their impact on insulin storage can seen as a serendipitous side effect of the evolution of the hormone within the β-cell environment, and its optimization for a particular, species specific, physiological profile.

It is also tempting to consider serotonin/dopamine-human insulin interactions as molecular fingerprints of insulin evolution in the animal kingdom, as insulin-like hormones are expressed in neurons in many invertebrates (54). The newly discovered (and still puzzling) role of insulin in the central nervous system, and the emergence of neuro-degeneration-linked so-called type III diabetes, thus places our findings in a much wider physiological context (55,56).

In summary, we show here that the insulin hexamer can act as a macromolecular sponge, keen to bind and assimilate a variety of physiological ligands and ions. This suggests that clinical exploration and use of insulin-hexamer stabilizing ligands, driven by steering of the pharmacokinetics of this hormone, may mirror its physiological canonical properties, rooted also in insulin evolution. Although the present work is aimed at shedding new light on the physiological storage state of this hormone, it may also open ways to novel approaches in medical formulations of insulin, toward its more desired closer to *in vivo* profile during subcutaneous injections administered in diabetes.

## EXPERIMENTAL PROCEDURES

*Molecular Dynamics Simulations* - All MD simulations were performed using the AMBER 14 program (57,58). In all simulations the AMBER ff03 protein force field (59) and SPC/E water model were used (60). Production simulations were performed in the isothermal-isobaric ensemble at ambient conditions of T = 300 K and p

= 1 atm using the Berendsen barostat and thermostat (61). The only exception were thermodynamic integration calculations, where the temperature was controlled by a Langevin thermostat with a reference temperature of T = 300 K and a collision frequency of 5 $ps^{-1}$ in order to avoid problems of non-ergodicity when the ligand is fully decoupled from its environment. 3D periodic boundary conditions were applied with a non-bonded interaction cutoff of 9 Å. The long-range electrostatic interactions were accounted for using the particle mesh Ewald method (62) using a cubic spline interpolation. The density of the charge grid was 64 × 64 × 64 and the direct sum threshold was $10^{-5}$. Van der Waals interactions beyond the cutoff were treated using the continuum model correction for energy and pressure. All bonds containing hydrogen atoms were constrained using the SHAKE algorithm (63). A time step of 2 fs was employed.

Mildly acidic conditions (pH ~ 5.5) of insulin storage granules would generally tend to favor a fully protonated side chain of HisB5 (64). However, due to zinc coordination the Nε2 atom of HisB10 is actually deprotonated (65,66). In addition, the six GluB13 side chains in the middle region of the insulin hexamer were considered as deprotonated. The overall charge of the protein is therefore −6. Initial simulations indicated diffusion of $Na^+$ cation/cations into the middle region. At least one $Na^+$ cation was always present in the middle region of the hexamer being placed to the middle region from the start of the simulation.

Substitution of the site I-bound phenol by the neurotransmitters serotonin or dopamine was also investigated. The $R_6$-state insulin complex with 6 phenols in sites I (referred to here as $InsPheR_6$) was used as a reference structure (PDB ID: 1AIY) due to a higher stability of this conformer and homogenous saturation of insulin hexamer with the same ligand (67). The starting structures for simulations were obtained by exchanging phenol molecules in site I by either dopamine or serotonin molecules with two initial conformations for each ligand. The ligands were built from the phenol core (1 oxygen atom and 6 carbon atoms) the structure of which was available from X-RAY structure). Subsequent restrained minimization eliminated any potential steric clashes. Starting geometries of phenolic ligands inside the phenolic pockets are depicted in Figure 2.

Phenol, serotonin, and dopamine were assigned parameters from ff03 AMBER force field using the ANTECHAMBER package (68). Both serotonin and dopamine have a charge of +1 e at pH 5.5. Partial atomic charges were obtained by the RESP method, calculated at the HF/6-31G+ level. These calculations were performed using the Gaussian 09 package (69).

The B10-Zn interaction potential had to be re-parametrized in order to account (at least partially) for the electronic polarization and charge transfer effects and thus to reproduce experimental data. The charges on zinc ions and on HisB10 were modified according to the results from *ab initio* calculations on small model systems to +1.5 e and +0.1677 e, respectively. These were obtained using the RESP/NPA analysis employing the B3LYP/aug-cc-pvtz level of theory. In a similar spirit, in order to account for electronic polarization effects in a mean-field way (70-73), we rescaled bulk $Na^+$ and $Cl^-$ (including the $Na^+$ cation located in the middle of the hexamer) ionic charges by a factor of 0.75.

Each of the liganded insulin $R_6$ hexamers was immersed into a unit cell containing 9 000 SPC/E water molecules, with $Na^+/Cl^-$ ions added to acquire overall electroneutrality with no excess of salt present. After preparation, the energy of each of the systems was minimized using 5 000 steps of the steepest descent method, where the protein and phenolic ligands were restrained with a harmonic potential. The systems were then subjected to 200 ps of isothermal-isochoric molecular dynamics, where the temperature was slowly raised from 10 to 300 K. This was followed by 1.2 ns of an isothermal-isobaric equilibration, which led to an equilibrated cell size of approximately 69 × 68 × 66 $Å^3$. Systems were assessed as equilibrated by monitoring temperature, cell size, density, and root mean square displacement of the protein. After equilibration, the production runs were propagated for 600 ns.

In addition to direct MD simulations free energy calculations employing the thermodynamic integration method were performed to determine apparent binding constants $K_d$ of phenol and the two neurotransmitters to the $R_6$ hexamer. The free energy cycles and further details of these simulations are presented in the SI. Similar free energy calculations for evaluation of the $K_d$ s to ligand binding sites III were performed using the

umbrella sampling methods (for more details see SI). Here, to stabilize the hexamer $R_6$ state, the site I was filled with phenol prior to the search for dopamine site III binding mode, as this neurotransmitter did not bind to site I in MD simulations.

*X-ray crystallography* - Crystallizations of all insulin complexes reported here were performed with the in-house insulin crystallization screens that cover most of previously reported crystal growth parameters. Crystallization conditions, data collection, refinement, and models statistics, as well as PDB codes are provided in Table S1. All crystals were directly flash-cooled in liquid $N_2$. X-ray data were collected at 100 K and processed by *xia2* (74), model building and refinement ($F>0\sigma F$) were performed by COOT (75) and the CCP4 suite of programs (76). Crystal structures were solved by Molrep (77) with the B1-B6 truncated insulin hexamer, hexamer-derived dimer, and insulin monomer as a model (based on PDB ID: 1MSO (78)), and refined by Refmac 5.8 ((79)). Figures were made using CCP4mg (80). For structural comparisons all insulin hexamer structures were superimposed in COOT by the SSM fit option. For comparison of site I ligand-binding modes, the relevant dimers were superimposed by Cα matching of the B9-19 helix for one of the monomers by the LSQ option in COOT.

*Determination of ligands' Kd values by a solution 4H3N assay* - Solution studies of the interactions of phenol, serotonin, dopamine, and arginine with porcine insulin were performed following protocols by Huang et al. (81), Bloom et al. (82), and Huus et al. (46). An anionic ligand 4H3N was used as a sensitive chromophoric probe to determine ligands' binding curves by monitoring UV/Vis absorption. 4H3N binds only in the insulin R-state (in the vicinity of HisB10), which red-shifts its absorption spectrum. The samples were dissolved in 10 mM K-phosphate buffer at pH 7.4. In all measurements porcine hexameric $Zn^{2+}$-insulin (two atoms of zinc per one hexamer) and 4H3N were used at 0.6 mM and 0.225 mM concentrations, respectively. Insulin was pre-incubated with 4H3N in a total volume 0.6 mL for 20 minutes at room temperature, after which a particular ligand (phenol, serotonin, dopamine, or arginine) was added in a minimum volume (0.6-3 μL) of 10 mM K-phosphate buffer. After 15 min of RT equilibration the UV/Vis absorbance spectra were collected on a Perkin Elmer, Lambda 25 UV/Vis Spectrometer (Massachusetts, USA). The spectra were taken in the range of 300-550 nm, and the difference spectra at $\lambda_{max}$ of 444 nm were obtained by subtracting the absorbance of ligand-free 4H3N from absorbance of ligand-bound 4H3N. The binding curves were analysed using a method of non-linear regression and a fitting program considering one-site specific binding with a Hill slope using GraphPad Prism 5.0. The final $K_d$, $B_{max}$, and $h$ values with standard errors were calculated from at least three independently determined binding curves for each system.

**Acknowledgement**: PJ thanks the Czech Science Foundation for support via grant no. 16-01074S. AMB, TG, CV, JJ and KK work was supported by the Medical Research Council (Grant MR/K000179/1 to AMB); we thank Diamond Light Source for access their beam lines (proposal numbers mx-7864 and mx-9948) that contributed to the results presented here. This work was also supported by the Research Project of the Czech Academy of Sciences RVO:61388963 (to the Institute of Organic Chemistry and Biochemistry). We thank Mr. Sam Hart for assistance with data collection, and Hayley Arthurs for crystallizations.

**Conflict of interest**: The authors declare that they have no conflicts of interest with the contents of this article.

**Author contributions**: VP carried out the MD simulations, CMV, MK and TRG carried our crystallographic experiments, KK and PH carried out solution 4H3N assays, JPT collected crystallographic data, AMB, PJ, JJ and LZ conceived the study, designed experiments and analyzed data. AMB, PJ and JJ wrote the paper. All authors discussed the results and commented on the manuscript.

## REFERENCES

1. Taniguchi, C. M., Emanuelli, B., and Kahn, C. R. (2006) Critical nodes in signalling pathways: insights into insulin action. *Nat. Rev. Mol. Cell. Biol.* **7**, 85-96
2. Cohen, P. (2006) Timeline - the twentieth century struggle to decipher insulin signalling. *Nat. Rev. Mol. Cell. Biol.* **7**, 867-873
3. Atkinson, M. A., Eisenbarth, G. S., and Michels, A. W. (2014) Type 1 diabetes. *Lancet* **383**, 69-82
4. Taylor, S. I., Accili, D., and Imai, Y. (1994) Insulin-resistance or insulin deficiency - which is the primary cause of Niddm. *Diabetes* **43**, 735-740
5. Turner, R. C., Hattersley, A. T., Shaw, J. T. E., and Levy, J. C. (1995) Type-Ii Diabetes - Clinical Aspects of Molecular Biological Studies. *Diabetes* **44**, 1-10
6. Giovannucci, E., Harlan, D. M., Archer, M. C., Bergenstal, R. M., Gapstur, S. M., Habel, L. A., Pollak, M., Regensteiner, J. G., and Yee, D. (2010) Diabetes and cancer: a consensus report. *CA: Cancer J. Clin.* **60**, 207-221
7. Vigneri, P., Frasca, F., Sciacca, L., Pandini, G., and Vigneri, R. (2009) Diabetes and cancer. *Endocr.-Relat. Cancer* **16**, 1103-1123
8. Cohen, D. H., and LeRoith, D. (2012) Obesity, type 2 diabetes, and cancer: the insulin and IGF connection. *Endocr.-Relat. Cancer* **19**, F27-F45
9. Arrieta-Cruz, I., and Gutierrez-Juarez, R. (2016) The role of insulin resistance and glucose metabolism dysregulation in the development of alzheimer s disease. *Rev. Invest. Clin.* **68**, 53-58
10. McKern, N. M., Lawrence, M. C., Streltsov, V. A., Lou, M. Z., Adams, T. E., Lovrecz, G. O., Elleman, T. C., Richards, K. M., Bentley, J. D., Pilling, P. A., Hoyne, P. A., Cartledge, K. A., Pham, T. M., Lewis, J. L., Sankovich, S. E., Stoichevska, V., Da Silva, E., Robinson, C. P., Frenkel, M. J., Sparrow, L. G., Fernley, R. T., Epa, V. C., and Ward, C. W. (2006) Structure of the insulin receptor ectodomain reveals a folded-over conformation. *Nature* **443**, 218-221
11. Lemmon, M. A., and Schlessinger, J. (2010) Cell signaling by receptor tyrosine kinases. *Cell* **141**, 1117-1134

12. Adams, M. J., Blundell, T. L., Dodson, E. J., Dodson, G. G., Vijayan, M., Baker, E. N., Harding, M. M., Hodgkin, D. C., Rimmer, B., and Sheat, S. (1969) Structure of rhombohedral 2 zinc insulin crystals. *Nature* **224**, 491-495
13. Dodson, G., and Steiner, D. (1998) The role of assembly in insulin's biosynthesis. *Curr. Opin. Struct. Biol.* **8**, 189-194
14. Mayer, J. P., Zhang, F., and DiMarchi, R. D. (2007) Insulin structure and function. *Biopolymers* **88**, 687-713
15. Ward, C. W., and Lawrence, M. C. (2011) Landmarks in insulin research. *Front. Endocrinol.* **2**, 76
16. Weiss, M. A. (2009) The structure and function of insulin: decoding the TR transition. in *Insulin and IGFs* (Litwack, G. ed.), Elsevier Academic Press, Inc., San Diego. pp 33-49
17. Menting, J. G., Whittaker, J., Margetts, M. B., Whittaker, L. J., Kong, G. K. W., Smith, B. J., Watson, C. J., Zakova, L., Kletvikova, E., Jiracek, J., Chan, S. J., Steiner, D. F., Dodson, G. G., Brzozowski, A. M., Weiss, M. A., Ward, C. W., and Lawrence, M. C. (2013) How insulin engages its primary binding site on the insulin receptor. *Nature* **493**, 241-245
18. Menting, J. G., Yang, Y. W., Chan, S. J., Phillips, N. B., Smith, B. J., Whittaker, J., Wickramasinghe, N. P., Whittaker, L. J., Pandyarajan, V., Wan, Z. L., Yadav, S. P., Carroll, J. M., Strokes, N., Roberts, C. T., Ismail-Beigi, F., Milewski, W., Steiner, D. F., Chauhan, V. S., Ward, C. W., Weiss, M. A., and Lawrence, M. C. (2014) Protective hinge in insulin opens to enable its receptor engagement. *Proc. Natl. Acad. Sci. U.S.A.* **111**, E3395-E3404
19. Derewenda, U., Derewenda, Z., Dodson, E. J., Dodson, G. G., Reynolds, C. D., Smith, G. D., Sparks, C., and Swenson, D. (1989) Phenol stabilizes more helix in a new symmetrical zinc insulin hexamer. *Nature* **338**, 594-596
20. Bentley, G., Dodson, E., Dodson, G., Hodgkin, D., and Mercola, D. (1976) Structure of insulin in 4-zinc insulin. *Nature* **261**, 166-168
21. Smith, G. D., Swenson, D. C., Dodson, E. J., Dodson, G. G., and Reynolds, C. D. (1984) Structural stability in the 4-zinc human insulin hexamer. *Proc. Natl. Acad. Sci. U.S.A.* **81**, 7093-7097
22. Brzovic, P. S., Choi, W. E., Borchardt, D., Kaarsholm, N. C., and Dunn, M. F. (1994) Structural asymmetry and half-site reactivity in the T to R allosteric transition of the insulin hexamer. *Biochemistry* **23**, 13057-13069
23. Smith, G. D., and Ciszak, E. (1994) The structure of a complex of hexameric insulin and 4'-hydroxyacetanilide. *Proc. Natl. Acad. Sci. U.S.A.* **91**, 8851-8855
24. Whittingham, J. L., Chaudhuri, S., Dodson, E. J., Moody, P. C., and Dodson, G. G. (1995) X-ray crystallographic studies on hexameric insulins in the presence of helix-stabilizing agents, thiocyanate, methylparaben, and phenol. *Biochemistry* **34**, 15553-15563
25. Smith, G. D., Ciszak, E., and Pangborn, W. (1996) A novel complex of a phenolic derivative with insulin: structural features related to the T->R transition. *Protein Sci.* **5**, 1502-1511
26. Dunn, M. F. (2005) Zinc-ligand interactions modulate assembly and stability of the insulin hexamer - a review. *Biometals* **18**, 295-303
27. Ciszak, E., and Smith, G. D. (1994) Crystallographic evidence for dual coordination around zinc in the T3R3 human insulin hexamer. *Biochemistry* **33**, 1512-1517
28. Smith, G. D. (1998) The phenolic binding site in T3R3f insulin. *J. Mol. Struct.* **470**, 71-80

29. Whittingham, J. L., Edwards, D. J., Antson, A. A., Clarkson, J. M., and Dodson, G. G. (1998) Interactions of phenol and m-cresol in the insulin hexamer, and their effect on the association properties of B28 pro --> Asp insulin analogues. *Biochemistry* **37**, 11516-11523
30. RahuelClermont, S., French, C. A., Kaarsholm, N. C., and Dunn, M. F. (1997) Mechanisms of stabilization of the insulin hexamer through allosteric ligand interactions. *Biochemistry* **36**, 5837-5845
31. Falck, B., and Hellman, B. (1963) Evidence for presence of biogenic amines in pancreatic islets. *Experientia* **19**, 139-140
32. Lundquist, I., Ekholm, R., and Ericson, L. E. (1971) Monoamines in pancreatic-islets of mouse - 5-hydroxytryptamine as an intracellular modifier of insulin-secretion, and hypoglycemic action of monoamine-oxidase inhibitors. *Diabetologia* **7**, 414-422
33. Ustione, A., Piston, D. W., and Harris, P. E. (2013) Minireview: dopaminergic regulation of insulin secretion from the pancreatic islet. *Mol. Endocrinol.* **27**, 1198-1207
34. Julius, D., Brake, A., Blair, L., Kunisawa, R., and Thorner, J. (1984) Isolation of the putative structural gene for the lysine-arginine-cleaving endopeptidase required for processing of yeast prepro-alpha-factor. *Cell* **37**, 1075-1089
35. Fricker, L. D., Evans, C. J., Esch, F. S., and Herbert, E. (1986) Cloning and sequence-analysis of cdna for bovine carboxypeptidase-E. *Nature* **323**, 461-464
36. Hagedorn, H. C., Jensen, B.N., Krarup, N. B., Wodstrup, I. (1936) Protamine insulinate. *JAMA-J. Am. Med. Assoc.* **106**, 177-180
37. Norrman, M., Hubalek, F., and Schluckebier, G. (2007) Structural characterization of insulin NPH formulations. *Eur. J. Pharm. Sci.* **30**, 414-423
38. Smith, G. D., Pangborn, W. A., and Blessing, R. H. (2001) Phase changes in T3R3f human insulin: temperature or pressure induced? *Acta Crystallogr. D.* **57**, 1091-1100
39. Bentley, G., Dodson, G., and Lewitova, A. (1978) Rhombohedral insulin crystal transformation. *J. Mol. Biol.* **126**, 871-875
40. Wagner, A., Diez, J., Schulze-Briese, C., and Schluckebier, G. (2009) Crystal structure of ultralente-a microcrystalline insulin suspension. *Proteins* **74**, 1018-1027
41. Steensgaard, D. B., Schluckebier, G., Strauss, H. M., Norrman, M., Thomsen, J. K., Friderichsen, A. V., Havelund, S., and Jonassen, I. (2013) Ligand-controlled assembly of hexamers, dihexamers, and linear multihexamer structures by the engineered acylated insulin degludec. *Biochemistry* **52**, 295-309
42. Smeekens, S. P., Avruch, A. S., Lamendola, J., Chan, S. J., and Steiner, D. F. (1991) Identification of a cdna-encoding a 2nd putative prohormone convertase related to Pc2 in Att20 cells and islets of Langerhans. *Proc. Natl. Acad. Sci. U.S.A.* **88**, 340-344
43. Smeekens, S. P., and Steiner, D. F. (1990) Identification of a human insulinoma cdna-encoding a novel mammalian protein structurally related to the yeast dibasic processing protease Kex2. *J. Biol. Chem.* **265**, 2997-3000
44. Brader, M. L., Kaarsholm, N. C., Lee, R. W. K., and Dunn, M. F. (1991) Characterization of the R-state insulin hexamer and its derivatives - the hexamer is stabilized by heterotropic ligand-binding interactions. *Biochemistry* **30**, 6636-6645
45. Choi, W. E., Brader, M. L., Aguilar, V., Kaarsholm, N. C., and Dunn, M. F. (1993) The allosteric transition of the insulin hexamer is modulated by homotropic and heterotropic interactions. *Biochemistry* **32**, 11638-11645

46. Huus, K., Havelund, S., Olsen, H. B., Sigurskjold, B. W., van de Weert, M., and Frokjaer, S. (2006) Ligand binding and thermostability of different allosteric states of the insulin zinc-hexamer. *Biochemistry* **45**, 4014-4024
47. Lisi, G. P., Png, C. Y. M., and Wilcox, D. E. (2014) Thermodynamic contributions to the stability of the insulin hexamer. *Biochemistry* **53**, 3576-3584
48. Seydoux, J., and Girardie.L. (1974) Evidence for 2 receptor areas in brown adipose-tissue (Bat). *Experientia* **30**, 683-683
49. Arakawa, T., Ejima, D., Tsumoto, K., Obeyama, N., Tanaka, Y., Kita, Y., and Timasheff, S. N. (2007) Suppression of protein interactions by arginine: A proposed mechanism of the arginine effects. *Biophys. Chem.* **127**, 1-8
50. Nuhu, M. M., and Curtis, R. (2015) Arginine dipeptides affect insulin aggregation in a pH- and ionic strength-dependent manner. *Biotechnol. J.* **10**, 404-416
51. Nicolson, T. J., Bellomo, E. A., Wijesekara, N., Loder, M. K., Baldwin, J. M., Gyulkhandanyan, A. V., Koshkin, V., Tarasov, A. I., Carzaniga, R., Kronenberger, K., Taneja, T. K., Xavier, G. D., Libert, S., Froguel, P., Scharfmann, R., Stetsyuk, V., Ravassard, P., Parker, H., Gribble, F. M., Reimann, F., Sladek, R., Hughes, S. J., Johnson, P. R. V., Masseboeuf, M., Burcelin, R., Baldwin, S. A., Liu, M., Lara-Lemus, R., Arvan, P., Schuit, F. C., Wheeler, M. B., Chimienti, F., and Rutter, G. A. (2009) Insulin storage and glucose homeostasis in mice null for the granule zinc transporter ZnT8 and studies of the type 2 diabetes-associated variants. *Diabetes* **58**, 2070-2083
52. Fava, E., Dehghany, J., Ouwendijk, J., Muller, A., Niederlein, A., Verkade, P., Meyer-Hermann, M., and Solimena, M. (2012) Novel standards in the measurement of rat insulin granules combining electron microscopy, high-content image analysis and in silico modelling. *Diabetologia* **55**, 1013-1023
53. Tsuboi, T., and Rutter, G. A. (2003) Multiple forms of "kiss-and-run" exocytosis revealed by evanescent wave microscopy. *Curr. Biol.* **13**, 563-567
54. Conlon, J. M. (2001) Evolution of the insulin molecule: insights into structure-activity and phylogenetic relationships. *Peptides* **22**, 1183-1193
55. Chami, B., Steel, A. J., De La Monte, S. M., and Sutherland, G. T. (2016) The rise and fall of insulin signaling in Alzheimer's disease. *Metab. Brain. Dis.* **31**, 497-515
56. Steen, E., Terry, B. M., Rivera, E. J., Cannon, J. L., Neely, T. R., Tavares, R., Xu, X. J., Wands, J. R., and de la Monte, S. M. (2005) Impaired insulin and insulin-like growth factor expression and signaling mechanisms in Alzheimer's disease - is this type 3 diabetes? *J. Alzheimers Dis.* **7**, 63-80
57. Case, D. A., Babin, V., Berryman, J.T., Betz, R.M., Cai, Q., Cerutti, D.S., Cheatham, T.E., Darden, T.A., Duke, R.E., Gohlke, A.W., Goetz, A.W., Gusarov, S., Homeyer, N., Janowski, P., Kaus, J., Kolossvary, I., Kovalenko, A., Lee, T.S., LeGrand, S., Luchko, T., Luo, R., Madej, B., Merz, K.M., Paesani, F., Roe, D.R., Roitberg, A., Sagui, C., Salomon-Ferrer, R., Seabra, G., Simmeling, C.L., Smith, W., Swails, J., Walker, R.C., Wang, J., Wolf, R.M., Wu, X., Kollman, P.A. (2014) AMBER 14, University of California, San Francisco
58. Salomon-Ferrer, R., Gotz, A. W., Poole, D., Le Grand, S., and Walker, R. C. (2013) Routine microsecond molecular dynamics simulations with AMBER on GPUs. 2. Explicit solvent particle mesh Ewald. *J. Chem. Theory Comput.* **9**, 3878-3888
59. Duan, Y., Wu, C., Chowdhury, S., Lee, M. C., Xiong, G. M., Zhang, W., Yang, R., Cieplak, P., Luo, R., Lee, T., Caldwell, J., Wang, J. M., and Kollman, P. (2003) A point-

charge force field for molecular mechanics simulations of proteins based on condensed-phase quantum mechanical calculations. *J. Comput. Chem.* **24**, 1999-2012
60. Berendsen, H. J. C., Grigera, J. R., and Straatsma, T. P. (1987) The missing term in effective pair potentials. *J. Phys. Chem.* **91**, 6269-6271
61. Berendsen, H. J. C., Postma, J. P. M., Vangunsteren, W. F., Dinola, A., and Haak, J. R. (1984) Molecular-dynamics with coupling to an external bath. *J. Chem. Phys.* **81**, 3684-3690
62. Essmann, U., Perera, L., Berkowitz, M. L., Darden, T., Lee, H., and Pedersen, L. G. (1995) A smooth particle mesh Ewald method. *J. Chem. Phys.* **103**, 8577-8593
63. Miyamoto, S., and Kollman, P. A. (1992) Settle - an analytical version of the shake and rattle algorithm for rigid water models. *J. Comput. Chem.* **13**, 952-962
64. Hutton, J. C. (1982) The internal pH and membrane-potential of the insulin-secretory granule. *Biochem. J.* **204**, 171-178
65. Ishikawa, T., Chatake, T., Morimoto, Y., Maeda, M., Kurihara, K., Tanaka, I., and Niimura, N. (2008) An abnormal pK(a) value of internal histidine of the insulin molecule revealed by neutron crystallographic analysis. *Biochem. Biophys. Res. Commun.* **376**, 32-35
66. Bryant, C., Spencer, D. B., Miller, A., Bakaysa, D. L., Mccune, K. S., Maple, S. R., Pekar, A. H., and Brems, D. N. (1993) Acid stabilization of insulin. *Biochemistry* **32**, 8075-8082
67. Chang, X. Q., Jorgensen, A. M. M., Bardrum, P., and Led, J. J. (1997) Solution structures of the R-6 human insulin hexamer. *Biochemistry* **36**, 9409-9422
68. Wang, J. M., Wang, W., Kollman, P. A., and Case, D. A. (2006) Automatic atom type and bond type perception in molecular mechanical calculations. *J. Mol. Graph. Model* **25**, 247-260
69. Frisch, M. J. T., G. W., Schlegel, H. B., Scuseria, G. E., Robb, M. A., Cheeseman, J. R., Scalmani, G., Barone, V., Mennucci, B., Petersson, G. A., Nakatsuji, H., Caricato, M., Li, X., Hratchian, H. P., Izmaylov, A. F., Bloino, J., Zheng, G., Sonnenberg, J. L., Hada, M., Ehara, M., Toyota, K., Fukuda, R., Hasegawa, J., Ishida, M., Nakajima, T., Honda, Y., Kitao, O., Nakai, H., Vreven, T., Montgomery, J. A., Jr., Peralta, J. E., Ogliaro, F., Bearpark, M., Heyd, J. J., Brothers, E., Kudin, K. N., Staroverov, V. N., Kobayashi, R., Normand, J., Raghavachari, K., Rendell, A., Burant, J. C., Iyengar, S. S., Tomasi, J., Cossi, M., Rega, N., Millam, J. M., Klene, M., Knox, J. E., Cross, J. B., Bakken, V., Adamo, C., Jaramillo, J., Gomperts, R., Stratmann, R. E., Yazyev, O., Austin, A. J., Cammi, R., Pomelli, C., Ochterski, J. W., Martin, R. L., Morokuma, K., Zakrzewski, V. G., Voth, G. A., Salvador, P., Dannenberg, J. J., Dapprich, S., Daniels, A. D., Farkas, Ö., Foresman, J. B., Ortiz, J. V., Cioslowski, J., Fox, D. J. (2009) Gaussian 09, Revision A. 1. Wallingford, CT
70. Leontyev, I., and Stuchebrukhov, A. (2011) Accounting for electronic polarization in non-polarizable force fields. *Phys. Chem. Chem. Phys.* **13**, 2613-2626
71. Leontyev, I. V., and Stuchebrukhov, A. A. (2012) Polarizable mean-field model of water for biological simulations with AMBER and CHARMM force fields. *J. Chem. Theory Comput.* **8**, 3207-3216
72. Leontyev, I. V., and Stuchebrukhov, A. A. (2014) Polarizable molecular interactions in condensed phase and their equivalent nonpolarizable models. *J. Chem. Phys.* **141**

73. Kohagen, M., Mason, P. E., and Jungwirth, P. (2016) Accounting for electronic polarization effects in aqueous sodium chloride via molecular dynamics aided by neutron scattering. *J. Phys. Chem. B* **120**, 1454-1460
74. Winter, G. (2010) xia2: an expert system for macromolecular crystallography data reduction. *J. Appl. Crystallogr.* **43**, 186-190
75. Emsley, P., and Cowtan, K. (2004) Coot: model-building tools for molecular graphics. *Acta Crystallogr. D* **60**, 2126-2132
76. Bailey, S. (1994) The Ccp4 suite - programs for protein crystallography. *Acta Crystallogr. D* **50**, 760-763
77. Vagin, A., and Teplyakov, A. (1997) MOLREP: an automated program for molecular replacement. *J. Appl. Crystallogr.* **30**, 1022-1025
78. Smith, G. D., Pangborn, W. A., and Blessing, R. H. (2003) The structure of T-6 human insulin at 1.0 angstrom resolution. *Acta Crystallographica Section D-Biological Crystallography* **59**, 474-482
79. Murshudov, G. N., Vagin, A. A., and Dodson, E. J. (1997) Refinement of macromolecular structures by the maximum-likelihood method. *Acta Crystallogr. D.* **53**, 240-255
80. McNicholas, S., Potterton, E., Wilson, K. S., and Noble, M. E. M. (2011) Presenting your structures: the CCP4mg molecular-graphics software. *Acta Crystallogr. D.* **67**, 386-394
81. Huang, S. T., Choi, W. E., Bloom, C., Leuenberger, M., and Dunn, M. F. (1997) Carboxylate ions are strong allosteric ligands for the HisB10 sites of the R-state insulin hexamer. *Biochemistry* **36**, 9878-9888
82. Bloom, C. R., Wu, N., Dunn, A., Kaarsholm, N. C., and Dunn, M. F. (1998) Comparison of the allosteric properties of the Co(II)- and Zn(II)-substituted insulin hexamers. *Biochemistry* **37**, 10937-10944

**FOOTNOTES**

[‡]Institute of Organic Chemistry and Biochemistry, Czech Academy of Sciences, v.v.i., Flemingovo nám 2, 166 10 Prague 6, Czech Republic.
[§]York Structural Biology Laboratory, Department of Chemistry, The University of York, Heslington, York YO10 5DD, United Kingdom.
[$]Current address: Department of Biochemistry, University of Geneva, Quai Ernest-Ansermet 30, 1205 Geneva, Switzerland.

This article contains supplemental Table S1 (X-ray data collection and refinement statistics), Table S2 (List of partial atomic charges of phenolic ligands used in this work), Table S3 (Entropy contribution to the free energy of binding of a phenol to the phenolic pockets), Table S4 (Entropy contribution to the free energy of binding of a phenolic ligand to binding site III), Fig. S1 (Electrostatic surface representation of insulin hexamers), Fig S2 (Scatter plot representation of the data shown in Table 3), Fig. S3 and S4 with the examples of ligand-related electron density maps for serotonin (Fig. S3) and for arginine (Fig. S4), Fig. S5 (Labelling of the phenolic ligands), Fig. S6 (A practical example of a complete thermodynamic cycle used to calculate the differences in the free energies of binding of phenolic ligands), and Figure S6

showing a complete thermodynamic cycle used to calculate the absolute free energy of binding of a phenol to R6 hexamer.

The structures of insulin complexes were deposited in PDB database under accession codes 5MAM, 5MT3, 5MT9.

**Table 1**. Standard free energies of binding of phenol, dopamine and serotonin, molecules to the binding site I (phenolic pocket), together with the corresponding dissociation constants.

| Ligand | $\Delta G_b°$ [kcal/mol] | $K_d$ [M] |
|---|---|---|
| Phenol | −4.49 ± 1.55 | $5.4 \times 10^{-4}$ |
| Dopamine | 1.10 ± 1.73 | 6.3 |
| Serotonin | −4.24 ± 1.87 | $8.1 \times 10^{-4}$ |

**Table 2.** Standard free energies of binding of phenol, dopamine and serotonin molecules to the binding site III and the corresponding dissociation constants. $W_0$ is free energy difference directly form umbrella sampling calculations, $\langle \Delta G_{symm} \rangle$ is hexamer symmetry contribution, $\Delta G_{vol}$ is volume entropy contribution (with respect to the standard state at 1 M), $\Delta G_b°$ is overall standard free energy of binding, and $K_d$ is the corresponding dissociation constant.

| Ligand in the binding site III | $W_0$ [kcal/mol] | $\langle \Delta G_{symm} \rangle$ [kcal/mol] | $\Delta G_{vol}$ [kcal/mol] | $\Delta G_b°$ [kcal/mol] | $K_d$ [M] |
|---|---|---|---|---|---|
| Phenol | −1.83 ± 0.28 | −0.36 | 1.38 ± 0.22 | −0.81± 0.36 | $2.59 \times 10^{-1}$ |
| Dopamine | −6.23 ± 0.67 | −0.36 | 3.2 ± 0.2 | −3.24± 0.70 | $4.38 \times 10^{-3}$ |
| Serotonin | −2.65 ± 0.55 | −0.36 | 2.0 ± 0.1 | −0.92± 0.56 | $2.13 \times 10^{-1}$ |

**Table 3.** Values of $K_d$, $B_{max}$ and Hill coefficient ($h$) for the interaction of phenol or serotonin with insulin hexamers in the presence of 4H3N and/or arginine and serotonin.

| Ligand | $K_d$ ± S.D. [mM] | $B_{max}$ ± S.D. | $h$ ± S.D. |
|---|---|---|---|
| Phenol (n = 4) | 0.86 ± 0.13 | 0.17 ± 0.01 | 2.22 ± 0.30 |
| Phenol and 5 mM Arg (n= 3) | 0.75 ± 0.01 | 0.10 ± 0.00 | 2.07 ± 0.19 |
| Phenol and 5 mM dopamine (n= 3) | 0.64 ± 0.06 | 0.13 ± 0.01 | 1.68 ± 0.18 |
| Serotonin (n= 3) | 3.34 ± 0.52 | 0.11 ± 0.08 | 1.63 ± 0.10 |
| Serotonin and 5 mM Arg (n= 3) | 3.12 ± 0.31 | 0.06 ± 0.00 | 2.64 ± 0.27 |
| Serotonin and 5 mM dopamine (n= 3) | 3.93 ± 1.28 | 0.05 ± 0.04 | 7.12 ± 7.50 |

**FIGURE 1.** General structural organization of the three main forms of insulin hexamer: $T_6$ (A), $T_3R^f_3$ (B) and $R_6$ (C) in the hexamer top view, along its 3-fold symmetry axis. Insulin B chains are in white, A chains are in pink; the chains of one, representative, insulin dimer are indicated in (A) in light blue (B-chains) and yellow (A-chains). Some N- and C-termini of one dimer are also indicated in (A) and only B-chain N-termini in (B) and (C), with * corresponding to the symmetry-related monomer within a dimer. The B1-B8 segments of the B-chains that contribute to the largest structural changes in TR transitions are in red (top of the hexamer), and in green (bottom of the hexamer). The $Zn^{2+}$ ion is in blue. (D), (E), (F): representative insulin monomers in T, $R^f$ and R-state, respectively, with a coloring code as in (A)-(C). Typical, main ligand binding sites I and III in the R insulin form are indicated in (C) as S1 and S3, respectively.

**FIGURE 2.** Starting conformations of phenol (A – insulin $R_6$ hexamer shown for the sake of clarity of the phenolic pocket location), serotonin (B), and dopamine (B) molecules (depicted by vdw spheres) in the phenolic site I pocket (amino acids A6 and A11 involved in the binding are depicted by a stick model); two initial orientations of serotonin, and dopamine were considered.

**FIGURE 3.** Root mean square deviations (rmsds) of the protein backbone (heavy atoms) from the insulin $R_6$ hexamer crystal structure with different phenolic ligands (phenol, dopamine, or serotonin). Labels (1) and (2) correspond to the two starting orientations of the neurotransmitter molecules.

**FIGURE 4.** Root mean square deviations (rmsds) from simulations of all phenolic ligands (serotonin or dopamine in two orientations) from the phenol binding pockets in the insulin $R_6$ hexamers (in total six phenolic ligands per one $R_6$ hexamer). Each line corresponds to the rmsd of one phenolic ligand from its starting position with respect to the O atom of CysA6/N of CysA11 involved in a hydrogen bond. A zero or small value of rmsd means a strong ligand - $R_6$ hexamer hydrogen bond, while a significant increase of rmsd indicates breaking of this bond.

**FIGURE 5.** Dopamine (top, red) and serotonin (bottom, magenta) spatial distributions around the insulin $R_6$ hexamer (top view). The A-/B-chains are in blue and yellow respectively; the same isodensity value (~50× the bulk concentration) was used for both neurotransmitters. Black circles depict the site III binding pockets.

**FIGURE 6.** Serotonin (top) and dopamine (bottom) binding site III formed by two adjacent insulin monomers (Chain A/A' and Chain B/B'). Detailed structures of amino acids involved in binding (GluA17 and TyrA14) are shown, too.

**FIGURE 7.** Free energy profiles of phenolic ligands entering the surface binding site III.

**FIGURE 8.** Serotonin binding sites in insulin $InsSerT_3R_3$ hexamer: top view (top), side view (bottom) of the hexamer (A-chains in pink, B-chains in white, $Zn^{2+}$ ions as blue spheres). Site I and III are indicated; some N-, C-termini of A/B-chains (T-state: T, R-state: R) are shown. Serotonin in atom-colored code, with C-atoms in yellow.

**FIGURE 9.** Serotonin binding sites: top - site I, bottom - site III, in insulin $InsSerT_3R_3$ complex (insulin colour code as in Fig 7, with side-chains C-atoms in green, water - red sphere). HBs - dashed lines, */R/T correspond to symmetry related dimer, and T/R-state of the monomer respectively. Strong HisB5-Nε2..p-pyrrole-centre contact is also shown.

**FIGURE 10.** Serotonin and arginine binding sites in insulin $InsSerArgT_3R_3$ hexamer: top view (top) and side view (bottom) of the hexamer (labeling and colour-coding as in Fig. 7, with arginine C-atoms in light green).

**FIGURE 11.** Arginine binding sites in the insulin InsSerArg$T_3R_3$ hexamer. Labeling and colour-coding as in Fig. 8, with $Cl^-$ ion as yellow.

**FIGURE 12.** Titration of insulin hexamers and 4H3N with phenol (A) or serotonin (B). Titration of insulin hexamers and 4H3N preincubated with 5 mM arginine with phenol (C) or serotonin (D). Titration of insulin hexamers and 4H3N preincubated with 5 mM dopamine with phenol (E) or serotonin (F). All measured binding curves are shown.

**FIGURE 1.**

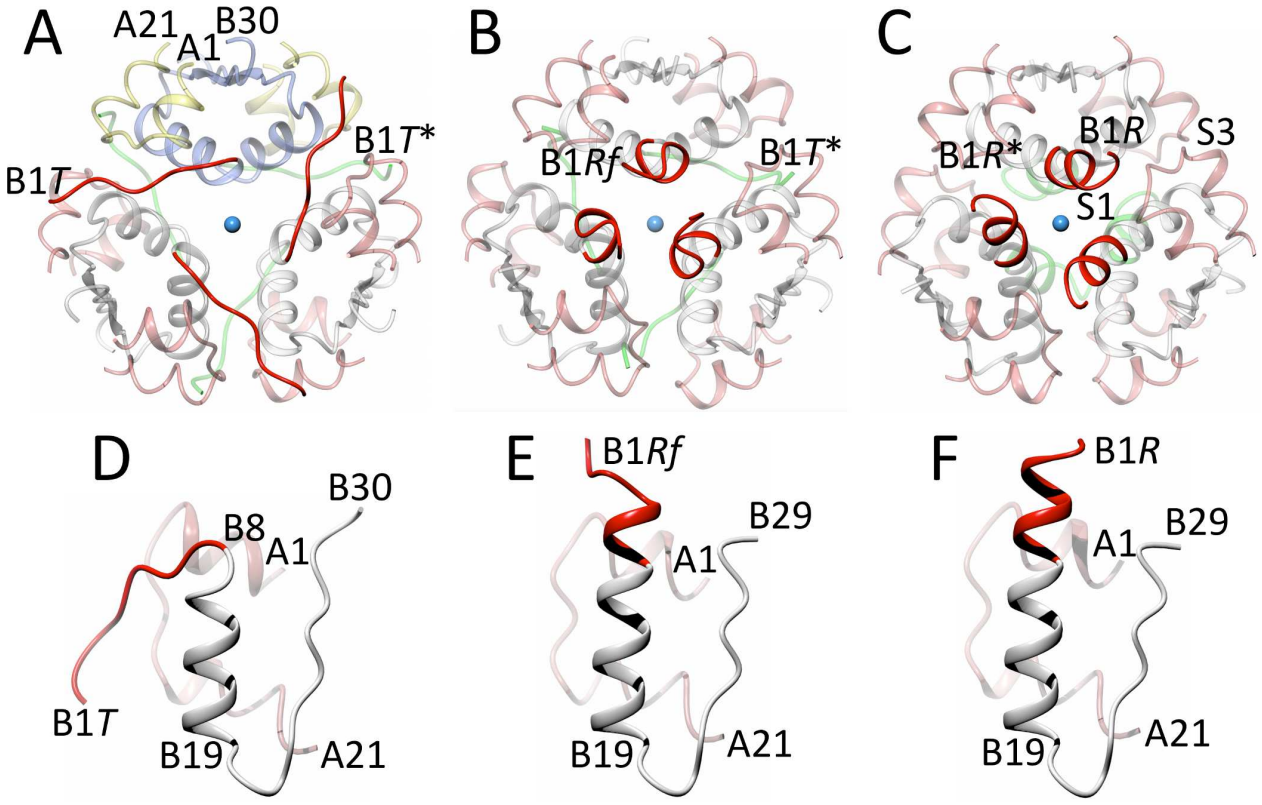
A
A21
A1
B30
B1T*
B1T
B
B1Rf
B1T*
C
B1R*
B1R
S3
S1
D
B30
B8
A1
B1T
B19
A21
E
B1Rf
B29
A1
B19
A21
F
B1R
B29
A1
B19
A21

**FIGURE 2.**

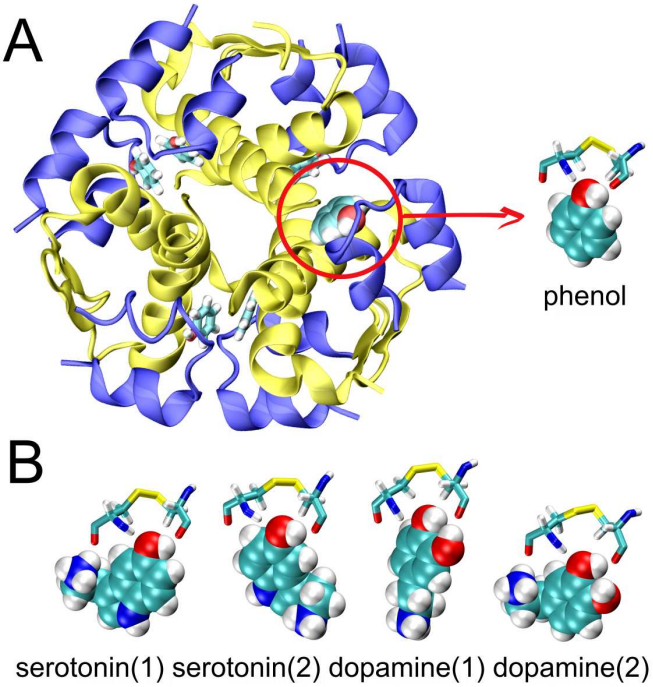

**FIGURE 3.**

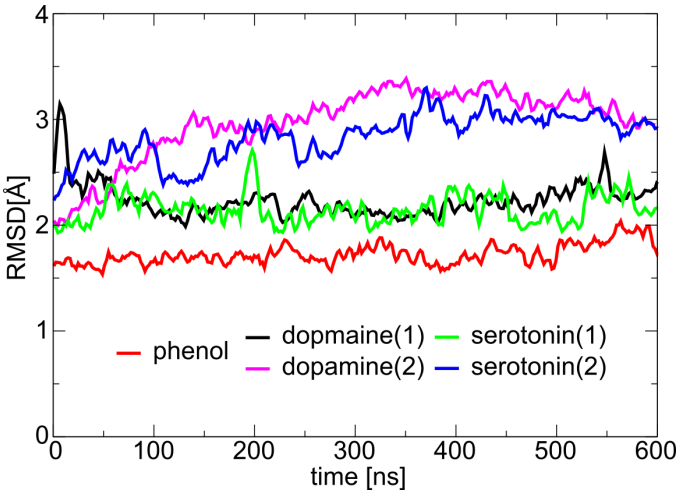
RMSD[Å]
time [ns]
phenol
dopmaine(1)
dopamine(2)
serotonin(1)
serotonin(2)
0
1
2
3
4
0
100
200
300
400
500
600

**FIGURE 4.**

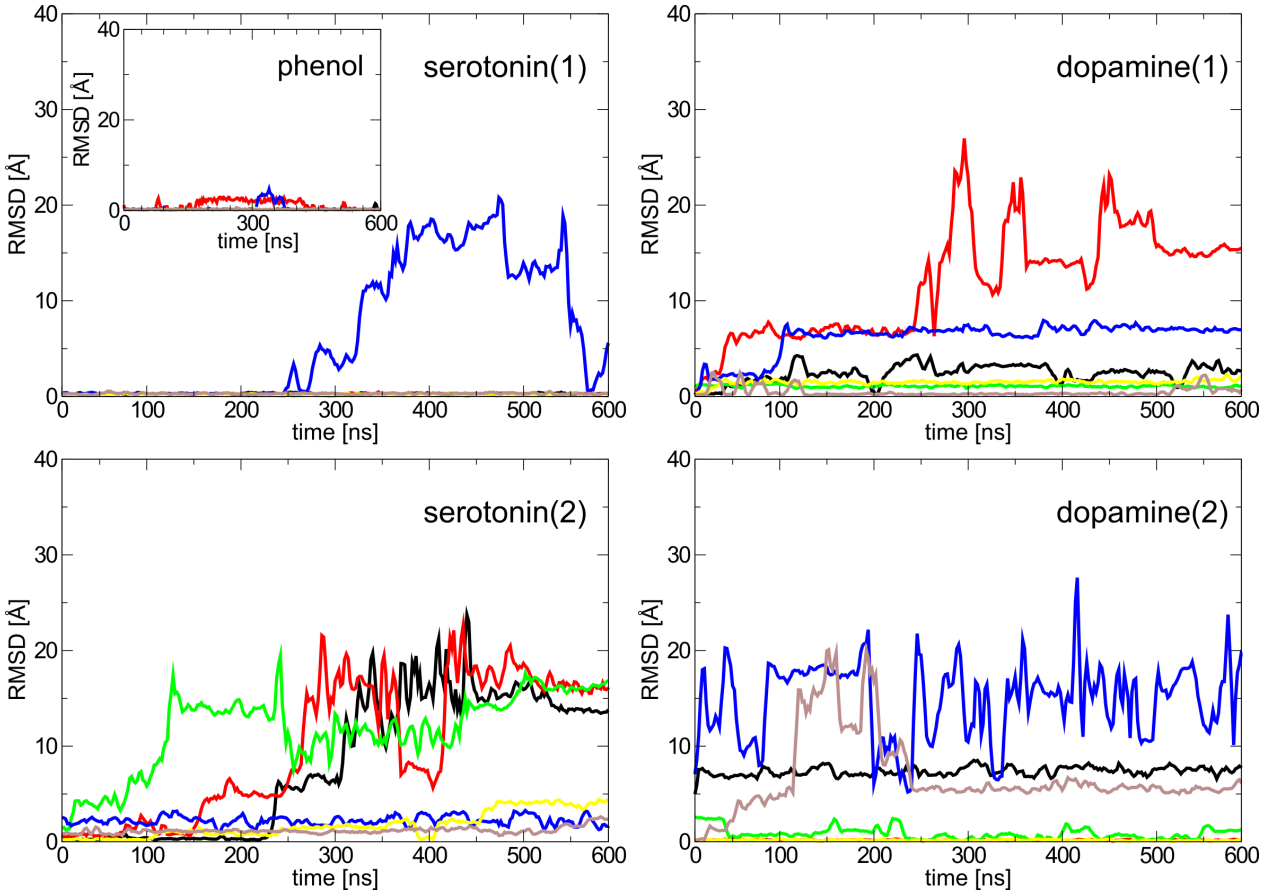
phenol
serotonin(1)
dopamine(1)
serotonin(2)
dopamine(2)
RMSD [Å]
time [ns]

**FIGURE 5.**

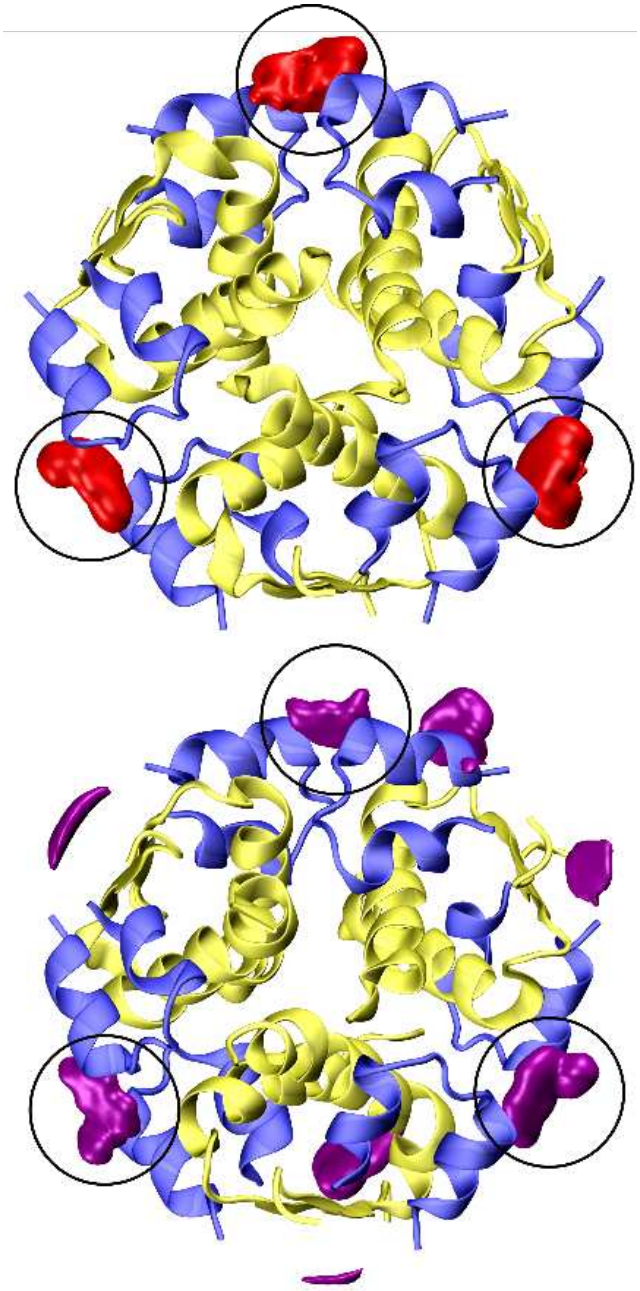

**FIGURE 6.**

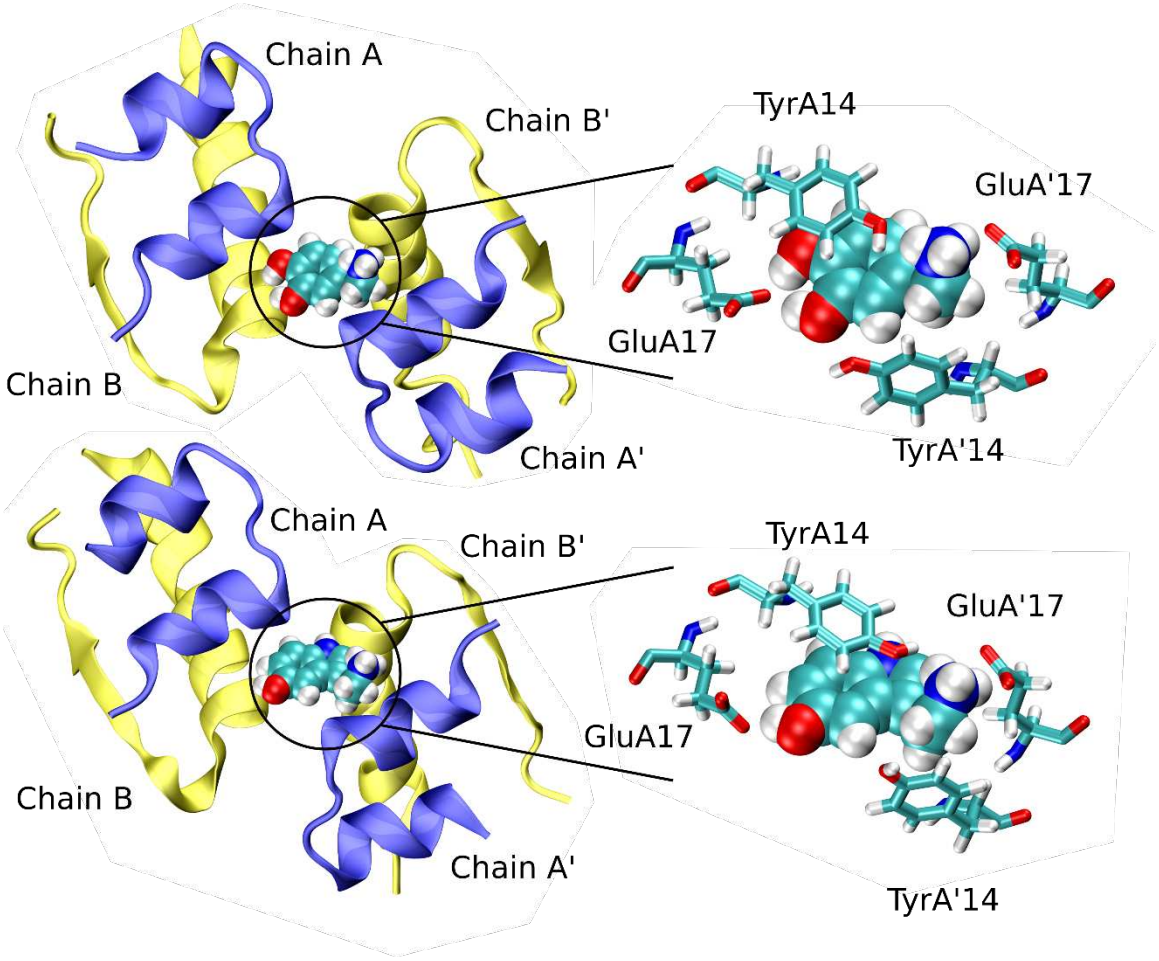
Chain A
Chain B'
TyrA14
GluA'17
GluA17
Chain B
Chain A'
TyrA'14
Chain A
Chain B'
TyrA14
GluA'17
GluA17
Chain B
Chain A'
TyrA'14

**FIGURE 7.**

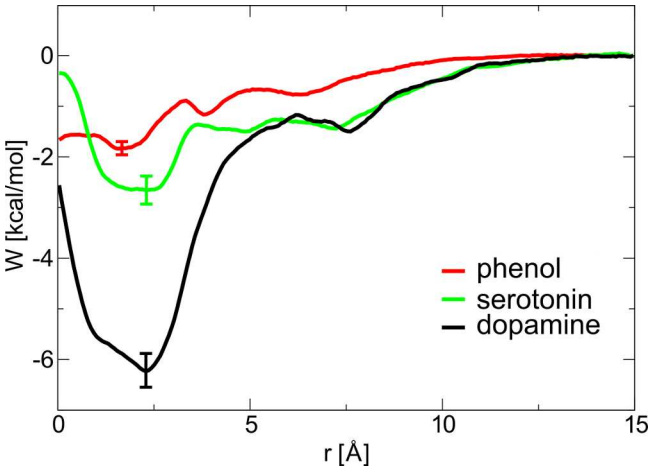

**FIGURE 8.**

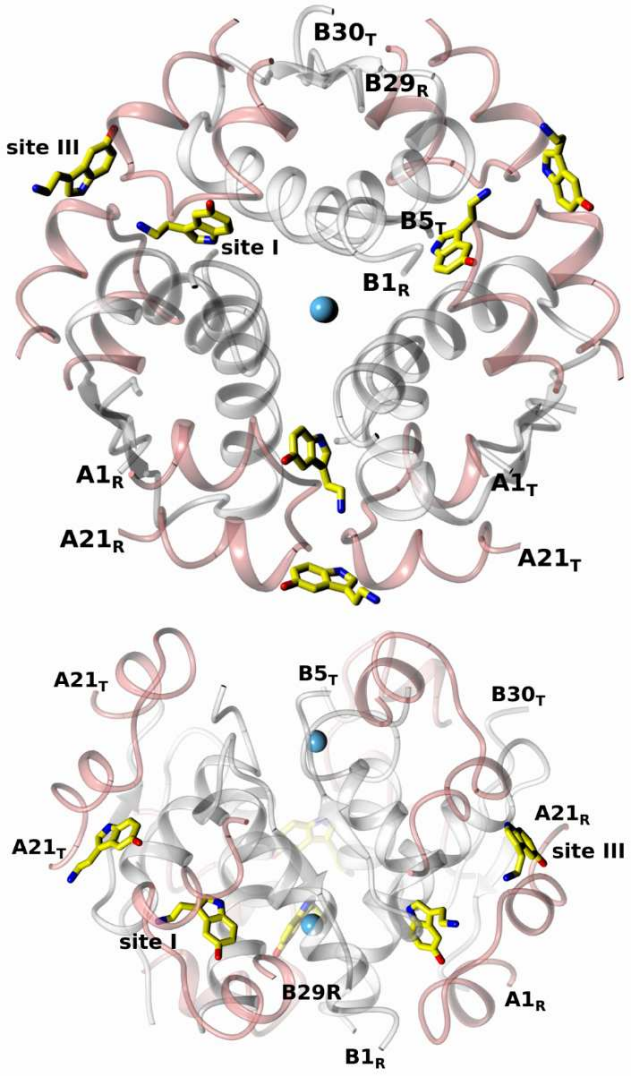
B30T
B29R
site III
B5T
site I
B1R
A1R
A1T
A21R
A21T
A21T
B5T
B30T
A21R
A21T
site III
site I
B29R
A1R
B1R

**FIGURE 9.**

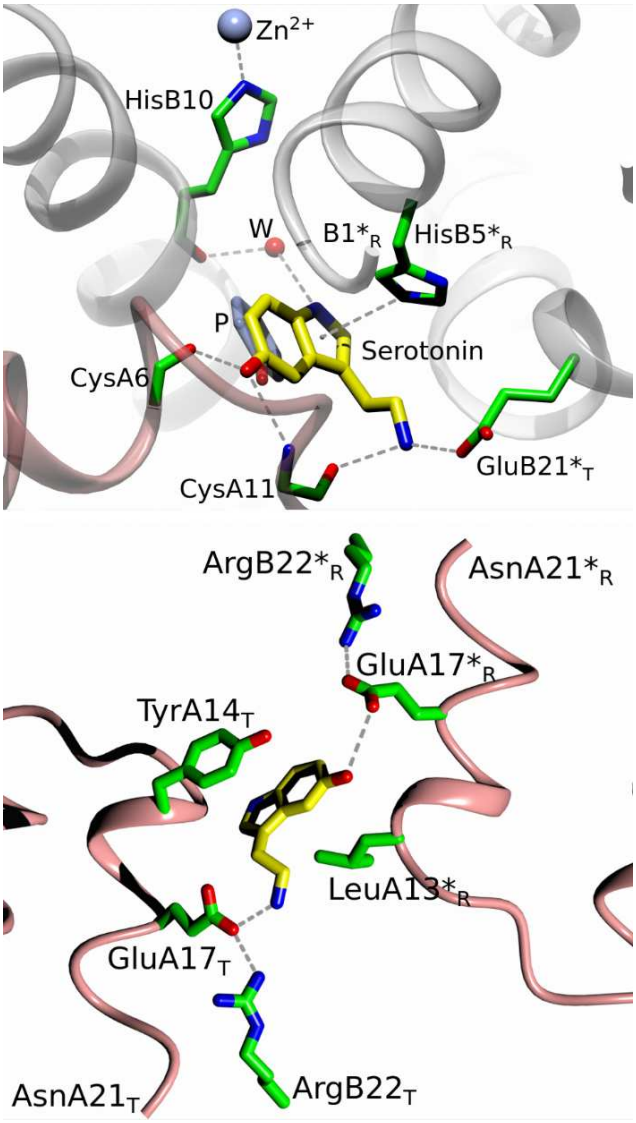
Zn2+
HisB10
W
B1*R
HisB5*R
P
Serotonin
CysA6
CysA11
GluB21*T
ArgB22*R
AsnA21*R
GluA17*R
TyrA14T
LeuA13*R
GluA17T
AsnA21T
ArgB22T

**FIGURE 10.**

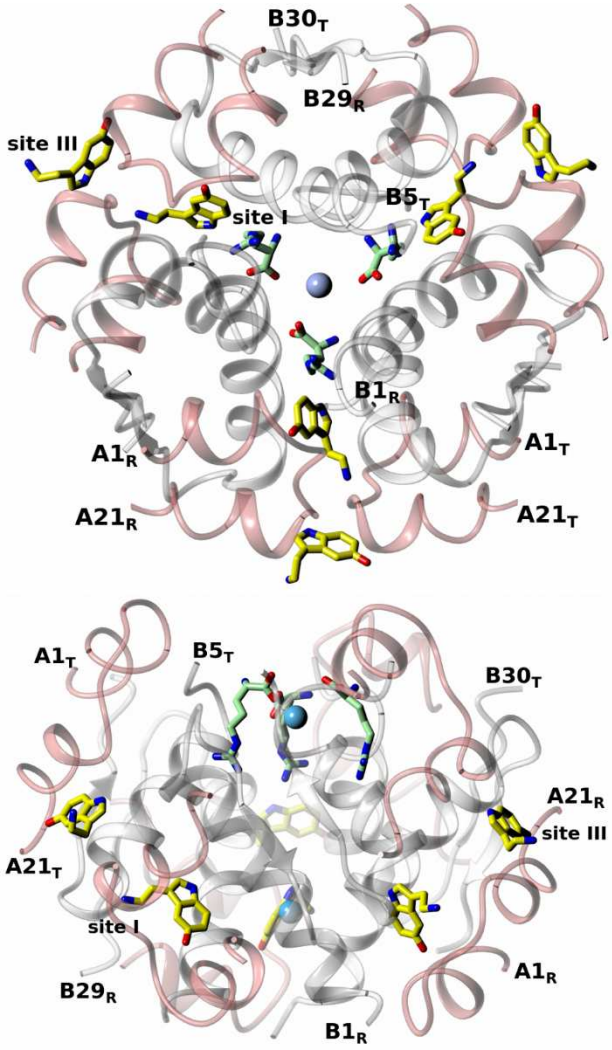
B30T
B29R
site III
B5T
site I
B1R
A1R
A1T
A21R
A21T
A1T
B5T
B30T
A21R
site III
A21T
site I
A1R
B29R
B1R

**FIGURE 11.**

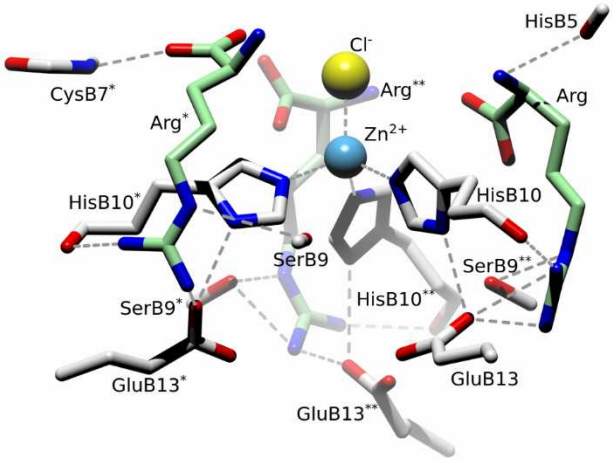
HisB5
Cl-
CysB7*
Arg**
Arg
Arg*
Zn2+
HisB10*
HisB10
SerB9
SerB9**
SerB9*
HisB10**
GluB13
GluB13*
GluB13**

**FIGURE 12.**

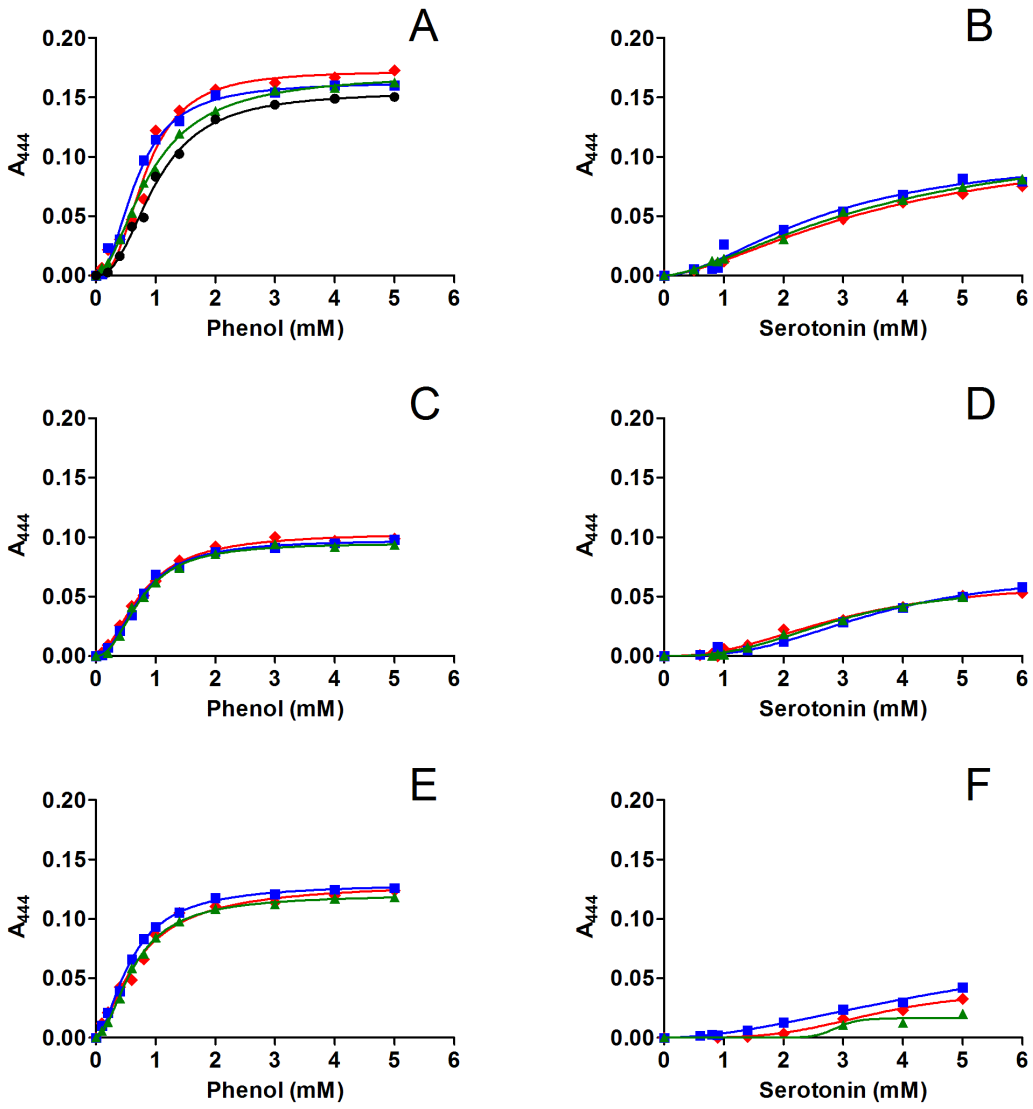
A
B
C
D
E
F
A444
0.20
0.15
0.10
0.05
0.00
0 1 2 3 4 5 6
Phenol (mM)
Serotonin (mM)